Monthly Notices
of the
ROYAL ASTRONOMICAL SOCIETY
MNRAS **467,** 27–49 (2017) doi:10.1093/mnras/stw3128

Interaction effects on galaxy pairs with Gemini/GMOS- III: stellar population synthesis

A. C. Krabbe,[1⋆] D. A. Rosa,[1⋆] M. G. Pastoriza,[2] G. F. Hägele,[3,4] M. V. Cardaci,[3,4] O. L. Dors, Jr[1] and C. Winge[2]

[1] *Universidade do Vale do Paraíba, Av. Shishima Hifumi 2911, Cep 12244-000, São José dos Campos, SP, Brazil*
[2] *Instituto de Física, Universidade Federal do Rio Grande do Sul, Av. Bento Gonçalves 9500, Cep 91359-050, Porto Alegre, RS, Brazil*
[3] *Instituto de Astrofísica de La Plata (CONICET La Plata–UNLP), Argentina*
[4] *Facultad de Ciencias Astronómicas y Geofísicas, Universidad Nacional de La Plata, Paseo del Bosque s/n, 1900 La Plata, Argentina*

Accepted 2016 November 30. Received 2016 November 25; in original form 2016 April 1

ABSTRACT

We present an observational study of the impacts of interactions on the stellar population in a sample of galaxy pairs. Long-slit spectra in the wavelength range 3440–7300 Å obtained with the Gemini Multi-Object Spectrograph (GMOS) at Gemini South for 15 galaxies in nine close pairs were used. The spatial distributions of the stellar population contributions were obtained using the stellar population synthesis code STARLIGHT. Taking into account the different contributions to the emitted light, we found that most of the galaxies in our sample are dominated by young/intermediate stellar populations. This result differs from the one derived for isolated galaxies, where the old stellar population dominates the disc surface brightness. We interpreted such different behaviour as being due to the effect of gas inflows along the discs of interacting galaxies on the star formation over a time-scale of the order of about 2 Gyr. We also found that, in general, the secondary galaxy of a pair has a higher contribution from the young stellar population than the primary one. We compared the estimated values of stellar and nebular extinction derived from the synthesis method and the Hα/Hβ emission-line ratio, finding that nebular extinctions are systematically higher than stellar ones by about a factor of 2. We did not find any correlation between nebular and stellar metallicities. Neither did we find a correlation between stellar metallicities and ages, while a positive correlation between nebular metallicities and stellar ages was obtained, with older regions being the most metal-rich.

Key words: galaxies: evolution – galaxies: interactions – galaxies: stellar content.

1 INTRODUCTION

Interactions and mergers of galaxies have a deep influence on the star formation pattern and on the chemical enrichment of the interstellar medium of these objects.

It is well known that interacting galaxies show enhanced star formation compared with isolated galaxies (e.g. Larson & Tinsley 1978; Sekiguch & Wolstencroft 1992; Donzelli & Pastoriza 1997; Barton, Geller & Kenyon 2003; Woods & Geller 2007; Scudder et al. 2012; Patton et al. 2013). Enhancement of the star formation rate (SFR) has been observed as being a function of the separation of close-pair galaxies. In fact, Patton et al. (2013), using spectroscopic data of about 211 000 star-forming galaxies taken from the Sloan Digital Sky Survey Data Release 7 (Abazajian et al. 2009), found a clear enhancement of the SFR for galaxies with projected separations up to 150 kpc, the strongest enhancements being for separations lower than ∼20 kpc (see also Barton, Geller & Kenyon 2000; Lambas et al. 2003; Nikolic, Cullen & Alexander 2004; Scudder et al. 2012; Casteels et al. 2013; Satyapal et al. 2014). The effect of the interaction on the SFR seems to be more pronounced for galaxy pairs that are low-mass (Woods & Geller 2007; Krabbe et al. 2008) and gas-rich (Chien et al. 2007).

SFR enhancements are accompanied by other events such as perturbations in the radial velocity field and dilution of the metallicity gradient. Interaction-induced flows of gas with low metallicity from the outer parts of the disc of a galaxy can decrease the metallicity in the inner regions and modify the radial abundance gradients. In fact, Krabbe et al. (2008), Kewley et al. (2010), Rupke, Kewley & Chien (2010) and Rosa et al. (2014), analysing spectroscopic data of H II

⋆ E-mail: angela.krabbe@gmail.com (ACK); deisearosa@gmail.com (DAR)

Table 1. Observed sample.

System name	Individual names	Designation	α (2000)	δ (2000)	PA (°)	$\Delta\lambda$ (Å)	$E(B-V)$	*NS* (kpc)
AM 1054–325	ESO 376–IG 027	AM 1054A	$10^h56^m58^s.2$	$-33^h09^m52^s$	77	4280–7130	0.084	–
	ESO–LV 37660271	AM 1054B	10 56 59.0	−33 09 39	77	4280–7130	0.083	17
AM 1219–430	ESO 267–IG 041	AM 1219A	12 21 57.3	−43 20 05	162,341	3350–7130	0.109	–
	FAIRALL 0157	AM 1219B	12 22 04.0	−43 20 21	25	3350–7130	0.110	33.7
AM 1256–433	ESO 269–IG 023 NED01	AM 1256B	12 58 57.6	−43 50 11	292,325	4280–7130	0.091	91.6
AM 1401–324	ESO 384–G 041	AM 1401A	14 04 14.7	−33 01 32	294,41	3350–6280	0.078	23.4
AM 2030–303	ESO 463–IG 003 NED01	AM 2030A	20 33 56.3	−30 22 41	75	4280–7130	0.070	–
	ESO 463–IG 003 NED02	AM 2030B	20 33 59.7	−30 22 29	75,22	4280–7130	0.060	–
	ESO 463–IG 003 NED03	AM 2030B	20 33 59.7	−30 22 23	22	4280–7130	0.060	40.5
AM 2058–381	ESO 341–G 030	AM 2058A	21 01 39.1	−38 04 59	42,125,350	3350–7130	0.050	–
	ESO 341–G 030 NOTES01	AM 2058B	21 01 39.9	−38 05 53	94,350	3350–7130	0.050	44
AM 2229–735	AM 2229–735 NED01	AM 2229A	22 33 43.7	−73 40 47	134,161	4280–7130	0.037	24.5
AM 2306–721	ESO 077–G 003	AM 2306A	23 09 39.3	−71 01 34	238,190	3350–7130	0.030	–
	ESO 077–IG 004	AM 2306B	23 09 44.5	−72 00 04	118,190	4280–7130	0.030	52.6
AM 2322–821	ESO 012–G 001, NGC 7637	AM 2322A	23 26 27.6	−81 54 42	59,28,318	3450–7130	0.181	–
	ESO 012–G 001 NOTES01	AM 2322B	23 25 55.4	−81 52 41	318	3350–7130	0.179	33.7

Notes. Column (1): system identification from the Arp–Madore catalogue (Arp & Madore 1987). Column (2): individual galaxy names from ESO/Uppsala catalogue (Lauberts 1982; Lauberts & Valentijn 1989), New General Catalogue (Dreyer 1888) and spectroscopic survey of southern compact and bright-nucleus galaxies of Fairall (1979). Column (3): adopted designation. Columns (4) and (5): equatorial coordinates for the centre of each observed galaxy. Columns (6)–(9): slit position angles, spectral wavelength coverage, $B-V$ colour excess and nuclear separation between components.

regions located in galaxy pairs, found shallow metallicity gradients. In particular, Rosa et al. (2014) found a break in the oxygen gradient (generally used as metallicity tracer) at a certain galactocentric distance in four interacting galaxies of their sample: AM 1219A, AM 1256B, AM 2030A and AM 2030B. Interestingly, these authors reported that the extreme SFR values estimated from the Hα emission-line fluxes (minimum SFR for AM1219A and AM2030B and maximum for AM 1256B and AM 2030) are located very close to the oxygen gradient break zones. Rosa and collaborators also suggested that, for the AM1219A and AM2030B systems, the minimum values of the SFR and break zone could be associated with corotation radii.

Determinations of SFR based on Hα emission-line fluxes give information on the ionizing star-forming clusters. To access the history of the stellar population, we should perform studies based on stellar population synthesis. Studies of the spatial distribution of the stellar population components in interacting galaxies yield important insights on the effects of the interaction on the kinematics of the galaxies involved, allowing us to know the periods during which bursts of star formation occurred, as well as the stage of the interaction (Krabbe et al. 2008).

In the previous articles of this series, we presented observational studies of the spatial variation of electron density (Krabbe et al. 2014, hereafter Paper I) and metallicity (Rosa et al. 2014, hereafter Paper II) of H II regions located in a sample of interacting systems of galaxies. In the present work, we used these data to obtain the stellar population across the discs of these galaxies and to study the impacts of the interaction on the stellar population of the galaxies in our sample. The main goals of our study are as follows.

(i) To estimate the main epoch of star formation along the disc of the interacting galaxies.

(ii) To analyse the relation between stellar population distributions and the metallicity of the gas phase.

(iii) To investigate the relation between the age of the dominant stellar population and several nebular parameters (e.g. metallicity, extinction).

This article is organized as follows. In Section 2, we summarize the observations and data reduction. In Section 3, the method used to perform the stellar population synthesis is described. Section 4 presents the detailed results of the stellar population synthesis. A discussion of our results is given in Section 5, while our conclusions are presented in Section 6.

2 OBSERVATIONAL DATA

The present study is based on long-slit spectroscopy of a sample of nine systems of galaxies in interaction, obtained with the Gemini Multi-Object Spectrograph (GMOS) attached to the 8-m Gemini South telescope. Spectra in the range of 3450–7130 Å were obtained with two settings with the B600 grating, a slit width of 1 arcsec and a spectral resolution of ∼5.5 Å. The blue setting provided wavelength coverage from 3450–6280 Å and the red setting 4280–7130 Å, both with about the same spectral resolution.

In Table 1 we listed basic information for the observed galaxies: the name of the galaxy system, the names of the individual galaxies, our abbreviated designations, the celestial equatorial coordinates (J2000), the slit position angles, the wavelength range of the spectra, the Galactic extinction $E(B-V)$ as listed in the NASA/IPAC Extragalactic Database (NED)[1] of each galaxy and the nuclear separation (NS) between the individual galaxies of the pairs. Detailed information about the galaxy systems and the slit positions observed for the objects in this sample was provided in Papers I and II, with the exception of the AM 1401–324 system, which was not included in the previous works because the wavelength coverage does not include the [N II] λ6584-Å emission line. For the AM 1401–324 system, the spectra were taken at two slit positions on the sky (PA = 294° and PA = 41°), with the goal of observing the nucleus and the brightest regions of the main galaxy of the system (see Fig. A1). The secondary galaxy of the AM 1401–324 system was not observed.

The data reduction followed the standard procedure and was discussed in detail in Papers I and II. Basically, the spectra comprise

[1] http://ned.ipac.caltech.edu/

the flux contained in an aperture of 1 × 1.152 arcsec^2, which, considering a spatially flat cosmology with $H_0 = 71$ km s^{-1} Mpc^{-1} (Wright 2006) and the distances to the systems of our sample (see Paper II), corresponds to apertures from ∼200 to ∼1100 pc on the galaxies plane. The spectra taken on red and blue settings were combined by applying a median filter with the IRAF task LSCOMBINE.

3 STELLAR POPULATION SYNTHESIS

In order to obtain the stellar population contribution of our sample of interacting galaxies, we used the STARLIGHT stellar population synthesis code (Cid Fernandes et al. 2004, 2005, 2007; Mateus et al. 2006; Asari et al. 2007), which is discussed in detail in Cid Fernandes et al. (2004, 2005). Briefly, the code fits the observed spectrum (O_λ) of a galaxy using a combination of simple stellar populations (SSPs) obtained from evolutionary synthesis models by Bruzual & Charlot (2003). These models are composed of spectra with a resolution of 3 Å across the wavelength range 3200–9500 Å with a wide range of metallicities. STARLIGHT assumes the Padova 1994 tracks, as recommended by Bruzual & Charlot (2003), and an initial mass function (IMF) by Chabrier (2003) for stars with masses between 0.1 and 100 $M_\odot$.

The synthetic spectrum M_λ is solved by STARLIGHT according to the following equation:

$$M_\lambda = M_{\lambda_0}\left[\sum_{j=1}^{N_\star} \boldsymbol{x}_j b_{j,\lambda} r_\lambda\right] \otimes G(v_\star, \sigma_\star), \quad (1)$$

where $b_{j,\lambda}$ is the reddened spectrum of the jth SSP normalized at $\lambda_0 = 5870$ Å; $r_\lambda \equiv 10^{-0.4(A_\lambda - A_{\lambda_0})}$ is the extinction term; $\otimes$ represents the convolution operator; $G(v_\star, \sigma\star)$ is the Gaussian distribution used to model the line-of-sight stellar motions, centred at velocity $v_\star$ and with a dispersion $\sigma_\star$; M_{λ_0} is the synthetic flux at the normalization wavelength; and $\boldsymbol{x}$ is the population vector. The population vector represents the fractional contribution of the SSPs in terms of age and metallicity (t_j, Z_j) over the synthetic flux at λ_0. These spectral components can also be expressed as a function of the mass of the population, represented by the vector $\boldsymbol{m}$.

The fit between the observed and modelled spectra is calculated with the support of an algorithm that searches for the minimum value of

$$\chi^2(x, v_\star, \sigma\star, A_V, M_{\lambda_0}) = \sum_{\lambda=1}^{N_\lambda}[w_\lambda(O_\lambda - M_\lambda)]^2, \quad (2)$$

where w_λ^{-1} is the error in O_λ. Emission lines and spurious pixels are excluded from the fits, establishing $w_\lambda = 0$. The intrinsic reddening is modelled by STARLIGHT as due to foreground dust, using the extinction law of Cardelli et al. (1989), with $R_V = 3.1$ and parametrized by the V-band extinction, $A_V = R_V E(B - V)$. The SSPs considered in this work take into account 15 ages, $t = 0.001$, 0.003,0.005, 0.01, 0.025, 0.04, 0.1, 0.3, 0.6, 0.9, 1.4, 2.5, 5, 11 and 13 Gyr, and three metallicities, $Z = 0.2$, 1 and 2.5 $Z_\odot$, summing up $N_\star = 45$ SSP components. The stellar spectra of the SSPs were convolved with an elliptical Gaussian function to achieve the same spectral resolution as the observed one, transformed into the rest frame, normalized to λ5870 Å and corrected by foreground Galactic extinction as in Schlegel, Finkbeiner & Davis (1998).

The STARLIGHT code provides individual population vectors. However, according to Cid Fernandes et al. (2005), the individual components of $\boldsymbol{x}$ are very uncertain. To troubleshoot this problem, Cid Fernandes et al. (2005) proposed that the population contribution should be combined in age bins. Following the prescription of these authors, the population vectors are binned according to the flux contribution into young, x_y ($t \leq 4 \times 10^7$ years), intermediate-age, x_i ($4\times 10^7 < t \leq 2.5 \times 10^9$ years), and old, x_o ($t > 2.5 \times 10^9$ years) components, which have uncertainties lower than 0.05, 0.1 and 0.1, respectively, for signal-to-noise ratio S/N > 10. The same bins are to be used for the fractional contribution to the stellar mass $\boldsymbol{m}$ (m_y, m_i, m_o). The quality of the fitting result is quantified by the parameters χ^2 and *adev*. The latter gives the relative mean deviation $|(O_\lambda - M_\lambda)|/O_\lambda$ over all fitted pixels between the observed and model spectra.

4 RESULTS

In Table 2, the stellar population results are presented for the regions located along the disc of each galaxy in our sample. These regions are the same as considered in Papers I and II. Fig. 1 shows an example of the results of the synthesized spectrum and the pure emission for the nuclear region of AM 1219A and AM 1219B, while the results for the nuclear regions of the other objects in our sample are shown in Appendix F (Figs F1 and F2). The results of the synthesis are summarized in Table 2 for the individual spatial bins in each galaxy, stated as the percentage contribution of each base element weighted by flux and mass. In Fig. 2, the contribution of the stellar population components along the slit position of AM 1054A and AM 1054B is shown. The nominal centre of each slit was chosen to be the continuum peak at λ5870-Å flux. The remaining synthesis results are shown in Appendix F (Figs F3–F11), where the regions with intersection at the spectrograph slit positions are highlighted in the plots by different fill patterns. In Fig. 3, the synthesis results for AM 1219A and AM 1256B are plotted as a function of the galactocentric radius R normalized by R_{25} (galactocentric distance with surface brightness of 25 mag arcsec^{-2}; see table 2 of Paper II). In what follows, the results for each system are discussed separately.

4.1 AM 1054–325

This system is composed of a main spiral galaxy (hereafter AM 1054A) and a companion galaxy (hereafter AM 1054B). AM 1054A is an optically bright spiral in the early stages of merging (∼85 Myr; Mullan et al. 2011). As can be seen in Fig. 2 (top panel), the population synthesis results indicate that the light along the disc of AM 1054A is mainly dominated by a young stellar population component ($t \leq 4 \times 10^7$ yr), with a non-negligible contribution from an intermediate population. This spatial profile corresponds to a slit position crossing the supposed 'second' nucleus (or starburst region?) of AM1054 A (see Paper I).

In the bottom panel of Fig. 2, we can see that AM 1054B is mainly dominated by the old stellar population component, in the contribution of both light and mass, with a mean value of 62 per cent for light and 84 per cent for mass. The intermediate stellar population contributes significantly for this galaxy, with a mean value of about 30 per cent for a light-weighted context and 16 per cent for a mass-weighted one.

4.2 AM 1219–430

This system is composed of two galaxies, a main spiral galaxy (hereafter AM 1219A) and a secondary one (hereafter AM 1219B). The primary galaxy presents a normal arm to the south-west and a strong tidal arm, with several H II regions along it. AM 1219B has a bright nucleus with smooth open spiral arms. A bridge of material connecting both galaxies and a lens structure in addition

Table 2. Stellar population synthesis results for the AM 1054A galaxy. Results for the whole sample of galaxies are available in the electronic version.

Position (kpc)	x_y (per cent)	x_i (per cent)	x_o (per cent)	m_y (per cent)	m_i (per cent)	m_o (per cent)	χ^2	*adev*	A_V (mag)
				AM 1054A					
−0.564	80.3	13.9	0.5	52.9	39.0	8.1	0.8	4.54	0.37
−0.282	68.7	17.1	10.8	14.0	8.4	77.6	0.9	2.85	0.33
0.000	70.5	15.1	11.4	13.1	12.7	74.2	0.9	2.28	0.40
0.282	59.5	19.9	16.5	5.4	4.3	90.3	0.8	2.58	0.19
0.564	68.5	17.2	13.0	7.3	7.7	85.0	1.3	3.00	0.12
0.846	75.4	21.1	0.8	53.0	40.5	6.5	1.2	2.99	0.46
1.128	57.4	38.8	0.0	17.7	82.3	0.0	0.6	3.84	0.16
1.410	35.5	58.2	0.0	3.1	96.9	0.0	1.0	4.94	0.00
1.692	42.7	43.1	0.0	22.8	77.2	0.0	1.1	4.13	0.34
1.974	50.6	34.2	8.1	7.2	11.8	81.0	0.7	4.23	0.22

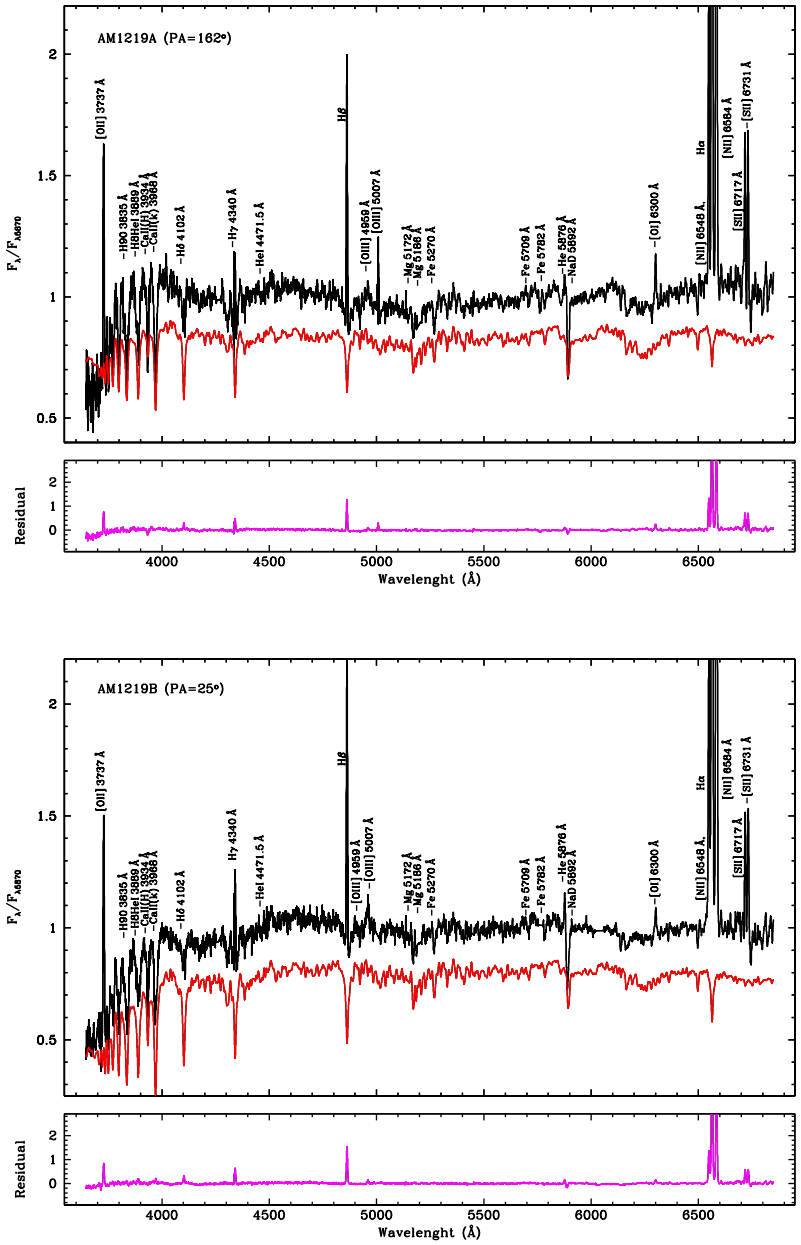

Figure 1. Stellar population synthesis for the nuclear region of AM 1219A and AM 1219B. For each object, we plotted in the top panel the observed (in black) and synthesized spectra (in red) and in the bottom panel the pure emission spectrum corrected for reddening. The main absorption and emission features have been identified.

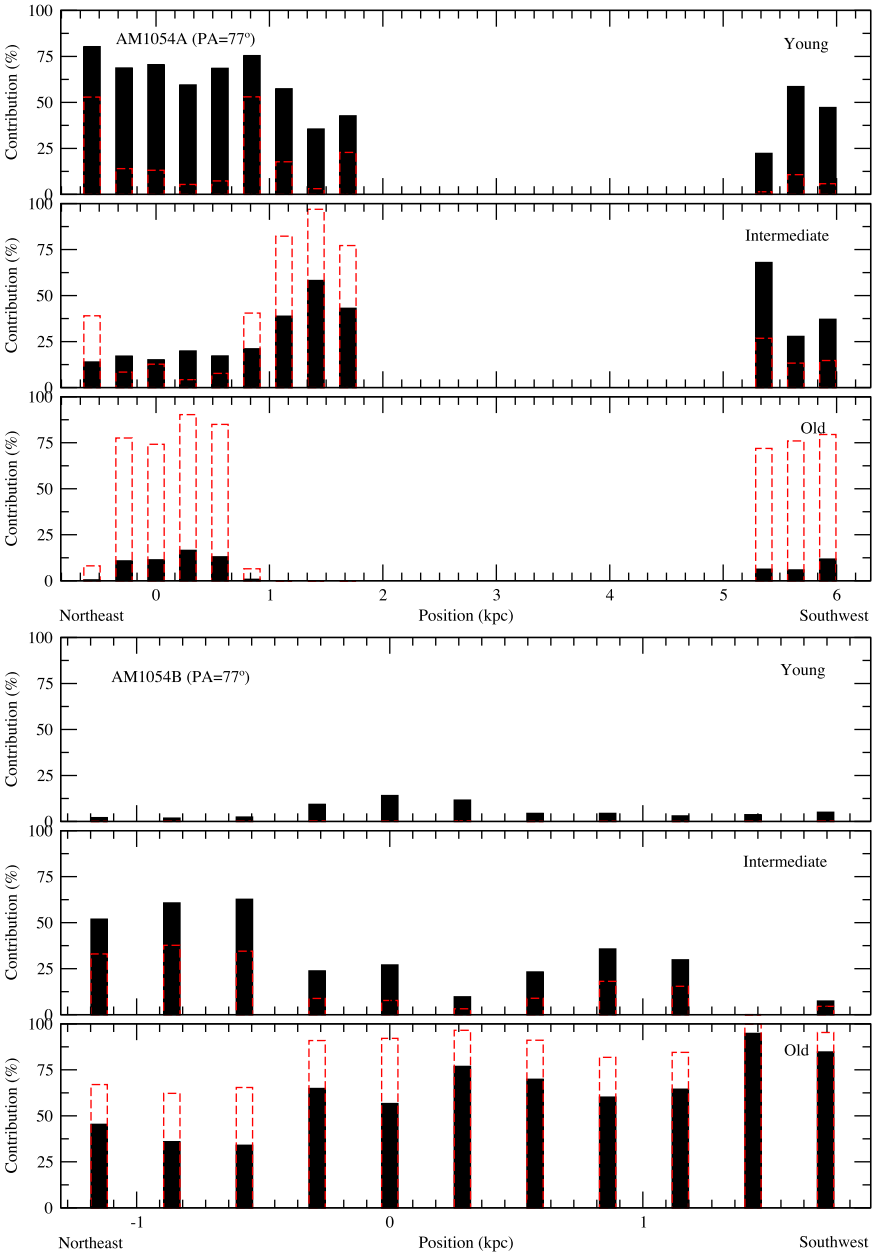

Figure 2. Synthesis results represented in terms of the flux (black) and mass fractions (red dashed) as a function of the distance to the centre of AM 1054A (top) and AM 1054B (bottom) along PA = 77°. For each object, the top panel corresponds to the young stellar population, the middle panel to the intermediate stellar population and the bottom panel to the old one.

to the bulge and disc of AM 1219B were reported by Hernandez-Jimenez et al. (2014). A rough estimate of the stellar population based on equivalent widths of absorption lines and on the continuum for the integrated spectrum of these galaxies shows that both components have a strong flux contribution from stellar populations younger than 10^8 years (Pastoriza, Donzelli J & Bonatto 1999). For the main galaxy, the estimations obtained in Paper I for electron densities show an increase of these towards the outskirts of this galaxy ($R/R_{25} \approx 0.5$). Interestingly, in this region an oxygen abundance break, which could be associated with a corotation radius, was obtained in Paper II.

The distribution of the stellar population in both galaxies is shown in Fig. F3. Three different slit positions were observed in AM 1219A: PA = 162° and PA = 341° along the north–south direction, crossing the nuclei and the disturbed arm, respectively, and PA = 70° in the north-east–south-west direction, crossing two very bright HII regions. For AM 1219B, we only have observations with PA = 25°crossing its nucleus.

For the slits with PA = 162° and PA = 70°, the light emitted by AM 1219A is dominated by the contribution of the young stellar component (∼54 per cent), with a significant contribution (∼35 per cent) from the old component. The intermediate stellar population is absent around the closest zone to the nucleus mapped by the slit with PA = 70°. This very bright zone (see fig. 1 of Paper II) corresponds to the continuum peak of an H II region complex. The stellar population spatial profile associated with this slit position seems to indicate an increase in the young stellar component towards this H II region complex. Considering the slit with PA = 341°, we

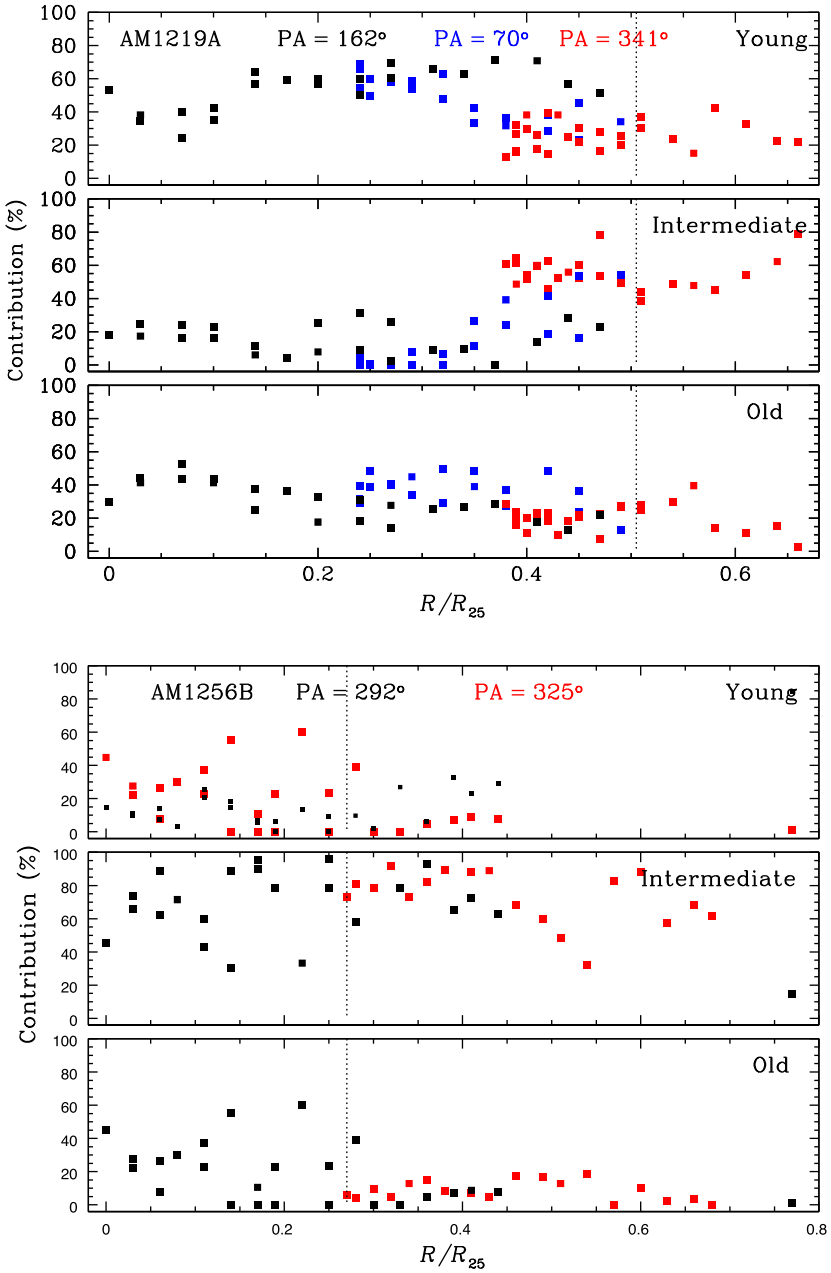

Figure 3. Synthesis results in terms of flux fraction as a function of galactocentric distance for AM1219A and AM1256B. Colours correspond to the different position angles.

can see that the intermediate stellar population dominates the light, with 56 per cent on average, followed by the young component, with 26 per cent on average. One possible interpretation of these results is that the intermediate stellar component could be associated with the perigalacticum passage. Preliminary estimations indicate that it occurred about 220 Myr ago (Hernandez-Jimenez et. al., private communication). Hence, along the disturbed arm, most of the stellar population could have been triggered during the perigalacticum passage, with a lower reservoir of gas remaining to form the younger generation of stars than in the other mapped parts of the galaxy, consequently decreasing the current star formation rate. As can be seen in Fig. 3, no variations of stellar population were found along PA = 341°. It is interesting to note that the zones sampled by two different slits, which are marked in Fig. F3, show estimations of their stellar population ages in reasonable agreement with each other.

The stellar population estimated for AM 1219B is roughly homogeneous along the observed slit. In terms of light-weighted fraction, the stellar population is distributed, on average, in three population components: 23 per cent young, 39 per cent intermediate and 40 per cent old.

Taking into account the contribution of different stellar populations to the mass, we found that in both components of this system the old stellar population is clearly the dominant component.

4.3 AM 1256–433

This system is composed of three galaxies, from which we only observed the secondary galaxy (hereafter AM 1256B). A break in the oxygen abundance gradient was obtained in Paper II at $R/R_{25} \approx 0.27$, which suggested that this break could be associated with a

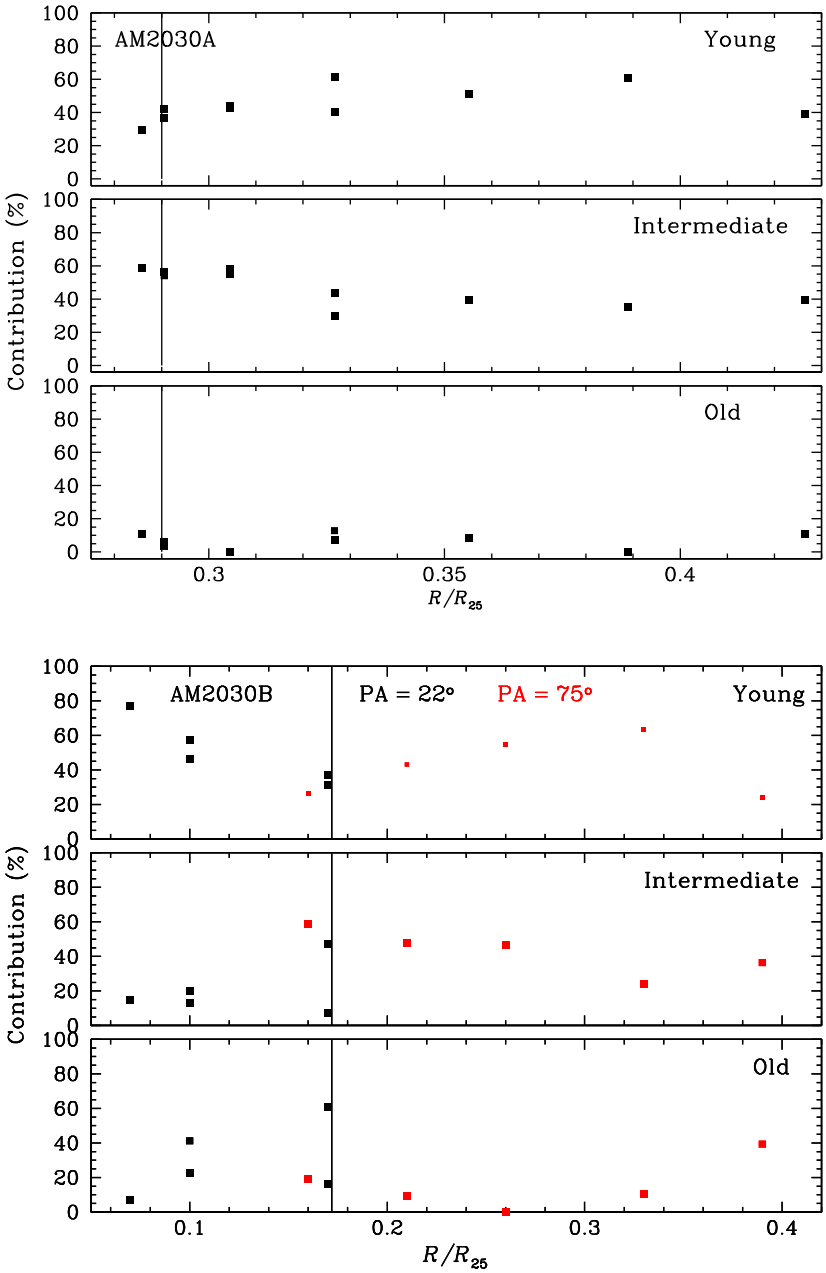

Figure 4. Same as Fig. 3, but for AM2030A and AM2030B.

corotation radius. Interestingly, at about the same position the maximum star formation rate was found (see Paper II).

As can be seen in Fig. F4, the stellar population is predominantly composed of the intermediate component, on average 70 per cent, for both slit positions. We observed variations of the stellar population across the galaxy, which in general are not dependent on position, with the exception of the region between 4 and 7 kpc along PA = 325°. In this region, the young component increases while the intermediate one decreases. This could probably be due to the slit not being completely aligned with the curved arm. In that area, the slit crosses the arm and therefore a young population is observed.

For PA = 292° and a distance of about 18 kpc from the centre of AM 1256B in the north-west direction (see fig. 1 of Paper I), there is a region where the young population represents about 80 per cent of the λ5870-Å flux. In this zone, there is an H II region with an age estimated by Ferreiro & Pastoriza (2004) of about 6 Myr, in agreement with our estimation. For this slit position, the light-dominant population is also mainly the intermediate one. In four cases, the old population contribution to the light is comparable to or even greater than that of the intermediate population. Analysing the mass contribution, we found that in the inner zone the old population dominates. The intersection of the spectrograph slit positions (marked in Fig. F4) shows stellar population estimations in good agreement, mainly for the light.

4.4 AM 1401–324

The main galaxy of this system, AM 1401A (ESO 384-G 041), has a very bright nucleus and an arm giving the appearance of a ring. Its companion is the smaller galaxy AM 1401B (ESO 384-G 041

NOTES01/PGC682060). Only the primary galaxy was observed. In Fig. A1 the slit positions are shown.

The results of the stellar population synthesis for AM 1401A are presented in Fig. F5. AM 1401A is completely light-dominated by intermediate stellar populations, with a contribution to the λ5870-Å flux of about 50–75 per cent in the central region and higher than 90 per cent in the outer regions. For the slit that crosses the nucleus (PA = 294°), there is a spatial variation of the stellar population and the light contribution of the intermediate one decreases towards the centre of the galaxy. The fraction of the old stellar population component is found to be increasing from the outer regions to the centre.

4.5 AM 2030–303

This is a system formed by a spiral galaxy as the main component (hereafter AM 2030A) and probably a triplet of irregular galaxies (see fig. 1 of Paper II) as the secondary component (hereafter AM2030B). Two different slit positions were used to acquired the data for this system: PA = 22° and PA = 75°. The first slit maps a complex of H II regions located in an outer arm of AM 2030A and crossing one of the irregular galaxies of AM 2030B. The second slit maps part of the secondary triplet complex.

For AM 2030A, we found a light-dominant stellar population with young/intermediate age, summing up more than 90 per cent of the optical flux at λ5870 Å (see Fig. F6). This result is expected, because the slit crosses a complex of H II regions, the age of which is estimated by Ferreiro & Pastoriza (2004) as about 6.5 Myr. As can be seen in Fig. F7, the AM 2030B spatial profile is derived mainly from two distinct regions along PA = 22°: one towards the north-east side and another towards the south-west, with measurements from ESO 463-IG 003 NED03 and ESO 463-IG 003 NED02, respectively. ESO 463-IG 003 NED03 is light-dominated by a young stellar population, with a significant contribution of the old stellar population in a couple of bins. On the other hand, ESO 463-IG 003 NED02 is light-dominated by an intermediate stellar population, with a significant contribution of old and young populations. For PA = 75°, the stellar population of AM 2030B is distributed mainly in young and intermediate populations. The spectra obtained from regions at the intersection of the slits presented low signal-to-noise ratios (S/N < 10) and therefore they were not used to perform the synthesis.

4.6 AM 2058–381

This system is composed of a two-arm spiral galaxy as the main component and an irregular one as the secondary, hereafter AM 2058A and AM 2058B respectively. The stellar population distributions in flux and mass of both components are shown in Fig. F8.

AM 2058A is dominated by an intermediate population component except for the inner zone, where the dominant component is the older one. For the slit positions that cross the centre of this galaxy (PA = 42° and PA = 350°), systematic variations are observed for the intermediate stellar component, i.e. its contribution to the flux is increasing outwards. On the other hand, a decrease in the older component can be seen in both contributions, flux and mass, from the centre to the outer regions. A small contribution (generally negligible) from the young population is observed. Along the spatial profile of PA = 125°, we found two two zones in which the young stellar component is prominent: one at ∼3 kpc towards the south-east and another at ∼7.5 kpc towards the north-west. As can be seen in fig. 1 of Paper I, these regions are located in one spiral arm and therefore we expect to observe a young population.

It can be seen in the bottom right panel of Fig. F8 that AM 2058B is dominated mainly by the contribution of the intermediate stellar population component in light as well as in mass, with mean values of 69 per cent and 74 per cent, respectively. No significant variations along the spatial profile are present in this galaxy.

4.7 AM 2229–735

AM 2229–735 is a system composed of a main spiral galaxy (hereafter AM 2229A) interacting with a smaller disc galaxy (hereafter AM 2229B). Spectra obtained along AM 2229B are very noisy (S/N ≪ 10) and they were not considered.

The contribution of the different stellar population components along the disc of AM 2229A for the two distinct slits is shown in Fig. F9. For both slit positions, there is a zone, the behaviour of which is noticeable. For PA = 161°, in the region between −4 and −8 kpc (hereafter called region A), the light and mass are mainly dominated by the young and intermediate populations. The same behaviour is shown by the zone between 0 and −3 kpc (hereafter called region B) for PA = 134°. These areas are marked in Fig. B1 and correspond to two complexes of H II regions. The origin of these complexes is probably related to interaction between the galaxies of this pair.

4.8 AM 2306–721

This pair is formed by a spiral galaxy (hereafter AM 2306A) and an irregular galaxy companion (hereafter AM2306B). As can be seen in Fig. F10, the optical fluxes of both galaxies are dominated mainly by the intermediate population component.

AM 2306A shows systematic variations for old and intermediate stellar components along the two slit positions observed. While the intermediate component is decreasing towards the centre of the galaxy, the old component is increasing. Likewise it can be seen that the young stellar population is increasing towards the outer regions of AM 2306A. This behaviour is more conspicuous for the regions mapped with the slit with PA = 238°, for which the more significant contributions from the young stellar component are located between −11 and −6 kpc and from 10–12 kpc, which corresponds to the regions on the spiral arms. Krabbe et al. (2008) derived the stellar population for this interacting system using the stellar population synthesis method developed by Bica (1998). This method employs the equivalent widths of several spectral absorption features and the measured continuum fluxes at different wavelengths, comparing them with those of a model computed from a base of simple stellar population (SSP) elements with known ages and metallicities. Our estimated stellar populations are in good agreement with the results previously obtained by Krabbe et al. (2008). In the case of the slit with PA = 190°, this increment towards the outer zones is also observed, although the variation of the light contribution from the young population is not so significant.

Interestingly, for AM2306B there is a completely different behaviour. Around the centre of this galaxy, we can see that the old stellar population dominates the mass content, although the intermediate and young populations dominate the light. Towards the north-west of the galaxy, there is a zone, between ∼3.5 and 8 kpc (PA = 118°), without an old stellar population component. At about 3 kpc, there is a zone for which the old stellar population dominates the mass content and around it (mapped by both slits) there are zones completely dominated (in mass and light) by the intermediate and

young stellar populations. Probably, this enhancement of stellar formation was triggered by the strong interaction with AM2306A.

4.9 AM 2322–821

The system AM 2322–821 (see fig. 1 of Paper II) is composed of a spiral galaxy classified as SA(r)c, showing disturbed arms (hereafter AM 2322A), in interaction with an irregular galaxy (hereafter AM 2322B). Four slit position angles were used to map this system: PA = 59° crossing the nucleus of AM2322A; PA = 28° crossing the main body of the primary but not across the nucleus (an offset of about 8 arcsec north-west, NW, from the nucleus); PA = 60° mapping the NW spiral arm of the main component, located between the main and secondary components; PA = 318° along the main axis of the secondary component AM 2322B and also along the north-east (NE) spiral arm of AM 2322A. As pointed out in Paper II, the spectra obtained using PA = 60° present low signal-to-noise ratio (S/N < 10). Therefore they were not used to perform the synthesis. Indeed, the spectra from the regions located in the intersections of the slits present low signal-to-noise ratio and therefore they were not considered in the synthesis.

The distribution of the stellar population in both galaxies of the AM 2322–821 system is shown in Fig. F11. The contribution to the light by the stellar populations is heterogeneous in AM 2322A for the three slit positions considered (PA = 28, 59, 318°). There are no hints of age gradients along this galaxy: the young, intermediate and old populations contribute significantly to the optical flux at λ5870 Å. It is worth noting that the mass is clearly dominated by the old stellar population component in the majority of the zones.

The light emitted by AM2322B is dominated by the young stellar population component in all of the galaxy except at its centre, where the contributions of the three populations are comparable. This young component shows a systematic variation along the slit, increasing outwards. In the outskirts, the old component barely contributes to the light, although it clearly dominates the mass all along the galaxy.

The stellar population in this system was studied by Krabbe et al. (2011) using the same data and a similar methodology to that in this work. Even though they considered four population-vector components, the results in both works are compatible. The contribution of the young population in AM 2322B was related to the perigalactic passage occurring at ∼90 Myr after perigalacticum (Krabbe et al. 2011).

5 DISCUSSION

5.1 Stellar population distribution

One of the main effects of interactions on the evolution of galaxies is to modify the stellar formation history of the objects involved. Our results, presented in the previous section, indicate that the light at λ5870 Å emitted by most of the galaxies in our sample is dominated by young/intermediate stellar populations, i.e. by stellar populations with ages lower than 2×10^9 years. A similar result was derived for other interacting galaxies by Dametto et al. (2014), who used near-infrared data to investigate the spatial distribution of the stellar populations in three interacting starburst galaxies. Indeed, young star clusters (ages lower than 300 Myr) have been found in tidal tails of interacting galaxies (e.g. Bastian et al. 2003; de Gris et al. 2003; Mulia, Chandar & Whitmore 2015). In contrast, in the discs of isolated galaxies the light is dominated by an older stellar population. In fact, Morelli et al. (2015) investigated the properties of the stellar populations in the discs of ten spiral galaxies, mostly not belonging to interacting systems. These authors found that the old stellar populations (ages higher than 4 Gyr) usually dominate the disc surface brightness. The difference in the light-dominant population between interacting and isolated galaxies could be due to the induced gas inflow, which increases the bursts of star formation along the disc during and after the interaction.

Another important issue is to investigate the differences between the stellar populations in the main and secondary galaxies belonging to interacting systems. Numerical simulations by Cox et al. (2008) showed that, during the interaction process in minor mergers, the fractional SFR enhancement is higher in the secondary galaxy, due to it being more susceptible to the tidal forces induced by the interaction. This theoretical result was confirmed by observational studies of the minor mergers AM 2306–721 by Krabbe et al. (2008) and NGC 7771+NGC 7770 by Alonso-Herrero et al. (2012). Inspection in Figs F8, F10 and F11 shows clearly that the secondary galaxies of the systems AM 2058–381, AM 2306–721 and AM 2322–821 have higher contributions of young stellar populations than the primary galaxies. For systems AM 1054–325 and AM 1219–430, an opposite result is derived (see Figs 2 and F3, respectively). However, the secondary galaxy of the system AM 1219–430 and the primary one of AM 1054–325 have few positions with available synthesis results. Moreover, only AM 1054B has an old population ($t > 2 \times 10^9$ years) as the main source of the flux at λ5870 Å. In fig. 1 of Paper I, we can see that this object has an elliptical form, the old population predominant being in it.

It is largely accepted that the growth of spiral galaxies follows the inside-out scenario, in the sense that inner regions of the disc are the most chemically evolved and present a higher percentage of old population than the outer regions (see e.g. Mólla & Díaz 2005; Brook et al. 2012; Few et al. 2012; Pilkington et al. 2012; Minchev et al. 2014). In fact, recently González Delgado et al. (2015), by using the data of the CALIFA survey (Sánchez et al. 2012), obtained the radial structure of the stellar population properties of 300 galaxies, mostly not interacting, and found negative age gradients, in agreement with an inside-out growth of galaxies. Other support for the assumption that spiral galaxies are formed following the inside-out scenario is that negative metallicity gradients are generally observed in isolated spiral galaxies (e.g. Pilyugin, Vílchez & Contini 2004; Dors & Copetti 2005; Sánchez et al. 2014; Pilyugin et al. 2015). For interacting galaxies, the metallicity gradients are modified by the gas flow and these objects present gradients significantly flatter than the ones observed in isolated galaxies (see e.g. Paper II and references therein). Moreover, it is unclear whether negative age gradients, which are the imprints of the inside-out scenario, are maintained in interacting galaxies.

In Figs C1–C3, the logarithm of the average of the stellar population age weighted by the light contribution of each population ($\log[\mathrm{Age_{light}}]$) versus the galactocentric distance R/R_{25} for our sample of objects is shown. $\mathrm{Age_{light}}$ gives information about the globally averaged star formation history in each galaxy (González Delgado et al. 2015). Taking into account the expected perturbations in a galaxy suffering stellar formation triggered by an external agent, we note that, for most spiral components (AM 1219A, AM 1256B, AM 1401A, AM 2058A, AM 2306A and AM 2322A) of the interacting pairs belonging to our sample, $\mathrm{Age_{light}}$ decreases with the increase of galactocentric distance, indicating that the interactions seem do not destroy the global imprints of galaxy formation, considering the inside-out scenario. AM 1054A and AM 2229A, both spiral galaxies, do not show this behaviour; however, for AM 1054A

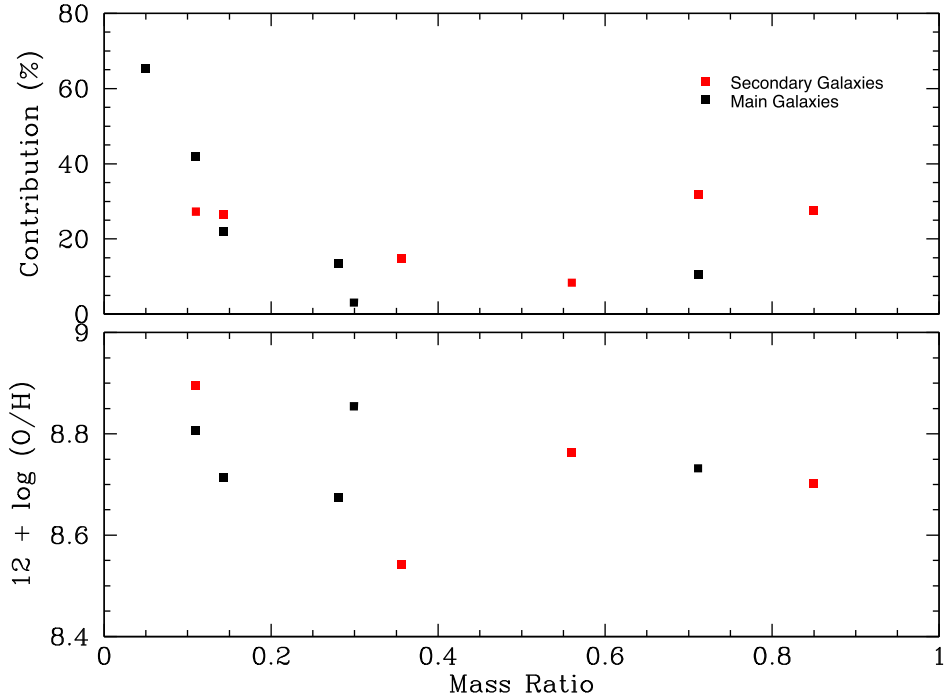

Figure 5. (Upper) Contribution of the young stellar population component to light and (lower) estimated oxygen abundance as a function of the mass ratio between the components ($M_{\rm secondary}/M_{\rm primary}$). Points represent the central region of the galaxies inside 1 kpc in diameter.

the slit crosses only their inner region and AM 2229A is a spiral, but very disturbed.

In Paper II, we found oxygen abundance breaks along the discs of galaxies AM 1219A, AM 1256B, AM 2030A and AM 2030B at galactocentric distances R/R_{25} between 0.2 and 0.5. In particular, for AM 1219A and AM 2030B we found a minimum in the instantaneous star formation rate (SFR) close to the break region and for AM 1256B and AM 2030A maximum values were derived. In particular, AM 1219A also presents a minimum value of the metallicity in the break region, which could be associated with a corotation radius, in agreement with the scenario proposed by Mishurov, Lépine & Acharova (2002). As can be seen in Fig. 3, we do not find variations of the stellar population associated with the corotation radius.

5.2 Stellar versus nebular extinction

The stellar population synthesis process gives us the extinction from the continuum, A_V[Synthesis]. We derive the nebular extinction A_V[Nebular] from the Hα/Hβ emission-line ratio, adopting the Calzetti, Kinney & Storchi-Bergmann (1994) law:

$$A_V[\text{Nebular}] = 7.96 \log \left[\frac{(\text{H}\alpha/\text{H}\beta)_{\rm obs}}{(\text{H}\alpha/\text{H}\beta)_{\rm int}} \right], \quad (3)$$

where $(\text{H}\alpha/\text{H}\beta)_{\rm obs}$ and $(\text{H}\alpha/\text{H}\beta)_{\rm int}$ are the observed and intrinsic ratios, respectively. We adopted the theoretical value of 2.86 for the intrinsic emission-line ratio (Osterbrock & Ferland 2006).

A comparison between the synthesis and the nebular extinctions is plotted in Fig. D1 and was performed for the objects in our sample. As can be seen in this figure, the nebular extinctions are higher than the stellar ones, up to about twice. These results are in agreement with those published earlier by Calzetti et al. (1994), Asari et al. (2007), Martins et al. (2013) and Dametto et al. (2014) and were interpreted by Calzetti et al. (1994) as a result of the fact that the hot (young) ionizing stars are associated with dustier regions than the cold stellar population.

5.3 Gas versus stellar parameters

We compared the nebular and stellar metallicities for our sample of galaxies, in order to search for a relation between these two quantities. We assume the oxygen abundance as a nebular metallicity estimator. For our sample, we estimated the oxygen abundances in Paper II using empirical calibrations based on strong emission lines and the stellar metallicity was obtained from the synthesis results.

Fig. E1 shows the nebular abundance versus stellar metallicity. As can be seen, there is no correlation between nebular and stellar metallicities. Similar results were found by Cacho et al. (2014) in a study of gaseous-phase metallicities and stellar populations in the centres of barred galaxies. In a study of stellar populations using Sloan Digital Sky Survey galaxies, Cid Fernandes et al. (2005) stated they had found a correlation between mass-weighted stellar metallicities and nebular oxygen abundances, although the dispersion is very large, with a Spearman rank correlation coefficient (R) of 0.48.

We also compared nebular and stellar metallicities as a function of stellar age. These comparisons are plotted in Fig. E2. As can be seen in the bottom panel of this figure, there is no correlation between stellar metallicities and stellar ages. In contrast, a relationship between nebular metallicities and stellar ages is found (see the upper panel of Fig. E2), in the sense that older regions are more metal-rich.

We analysed some properties of the nebular gas and the stellar populations belonging to the central region (1 kpc in diameter) of the galaxies. A comparison of the contribution (to the light) of the young stellar population component and the estimated oxygen abundances with the mass ratio between the components ($M_{\rm secondary}/M_{\rm primary}$) was performed (see the upper and lower panels of Fig. 5, respectively). The mass-ratio values were taken from Ferreiro & Pastoriza

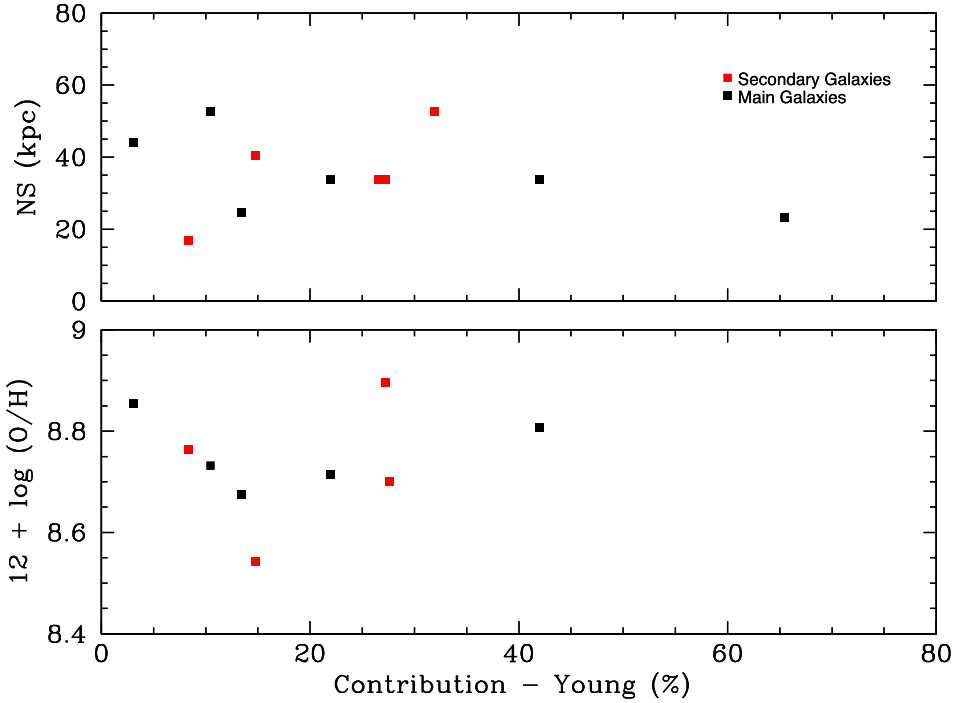

Figure 6. (Upper) Nuclear separation between pair components and (lower) estimated oxygen abundances as a function of the fraction of the young stellar population component to the light. Points represent the central region of the galaxies inside 1 kpc in diameter.

(2004). We also compared the nuclear separation between the components and the estimated oxygen abundances with the contribution (to the light) of the young stellar population component (see the upper and lower panels of Fig. 6, respectively). We did not find any correlation between the parameters studied. However, a more statistically significant sample is needed to reach any conclusive result.

6 CONCLUSIONS

We present an observational study of the stellar population in interacting galaxies using a synthesis method. Long-slit spectra in the spectral range 3440–7300 Å were obtained with the GMOS at Gemini South for 15 galaxies in nine close pairs. The stellar population contribution was obtained using the STARLIGHT stellar population synthesis code. The main results are summarized below.

(i) The contribution of the stellar components in relation to the optical flux at λ5870 Å for most of the galaxies in our sample – AM 1054A, AM 1219A, AM 1256B, AM 1401A, AM 2030A, AM 2030B, AM 2058A, AM 2058B, AM 2306A, AM 2306B and AM 2322B – is dominated by young/intermediate stellar populations.

(ii) No variations in the stellar population components were found for AM 1219A, AM 1256B, AM 2030A and AM 2030B at the oxygen-gradient break zones, which could be associated with corotation radii (see Paper II).

(iii) We compared the stellar extinction (A_V[Synthesis]) given by the population synthesis method with the nebular extinction (A_V[Nebular]) estimated from the Hα/Hβ emission-line ratio. We found that, for most of the objects, the nebular extinction is higher than the stellar extinction by up to about a factor of two.

(iv) No correlation was found between nebular and stellar metallicities.

(v) We compared the nebular and stellar metallicities as a function of stellar age. No correlation between stellar metallicities and stellar ages was found and a positive correlation between nebular metallicities and stellar ages was obtained, showing, as expected, that older regions are more metal-rich.

(vi) For the central regions of the galaxies studied, we did not find any correlation between the mass ratio and the contribution of the young stellar population component to the light or the estimated oxygen abundances. Neither did we find any correlation between the contribution of the young stellar population to the light and the nuclear separation of the pairs or the estimated oxygen abundances. However, more observations are needed to confirm these results.

ACKNOWLEDGEMENTS

Based on observations obtained at the Gemini Observatory, which is operated by the Association of Universities for Research in Astronomy, Inc., under a cooperative agreement with the NSF on behalf of the Gemini partnership: the National Science Foundation (United States), the Science and Technology Facilities Council (United Kingdom), the National Research Council (Canada), CONICYT (Chile), the Australian Research Council (Australia), Ministério da Ciencia e Tecnologia (Brazil) and SECYT (Argentina).

DAR thanks the support to PCI/MCTIC/INPE 300082/2016-9. OLD is grateful to the FAPESP and CNPq for supports under grants 2016/04728-7 and 306744/2014-7. ACK is thanks the FAPESP and CNPq for supports under grants 2016/21532-9 and 311826/2014-8, respectively.

REFERENCES

Abazajian K. N. et al., 2009, ApJS, 182, 543
Alonso-Herrero A. et al., 2012, MNRAS, 425, L46

Arp H. C., Madore B. F., 1987, A Catalogue of Southern Peculiar Galaxies and Associations 2 Volume Set, ISBN 0521343364. Cambridge University Press, Cambridge, 504 pp.
Asari N. V., Cid Fernandes R., Stasińska G., Torres-Papaqui J. P., Mateus A., Sodré L., Schoenell W., Gomes J. M., 2007, MNRAS, 381, 263
Barton E. J., Geller M. J., Kenyon S. J., 2000, ApJ, 530, 660
Barton G. E., Geller M. J., Kenyon S. J., 2003, ApJ, 582, 668
Bastian N., Hempel M., Kissler-Patig M., Homeier N. L., Trancho G., 2003, A&A, 435, 65
Bica E., 1998, A&A, 195, 9
Brook C. B. et al., 2012, MNRAS, 426, 690
Bruzual G., Charlot S., 2003, MNRAS, 344, 1000
Cacho R., Sánchez-Blázquez P., Gorgas J., Pérez I., 2014, MNRAS, 442, 2496
Calzetti D., Kinney A. L., Storchi-Bergmann T., 1994, ApJ, 429, 582
Cardelli J. A., Clayton G. C., Mathis J. S., 1989, ApJ, 345, 245
Casteels K. R. V. et al., 2013, MNRAS, 429, 1051
Chabrier G., 2003, PASP, 115, 763
Chien L., Barnes J. E., Kewley L. J., Chambers K. C., 2007, ApJ, 660, L105
Cid Fernandes R., Gu Q., Melnick J., Terlevich E., Terlevich R., Kunth D., Rodrigues Lacerda R., Joguet B., 2004, MNRAS, 355, 273
Cid Fernandes R., Mateus A., Sodré L., Stasińska G., Gomes J. M., 2005, MNRAS, 358, 363
Cid Fernandes R., Asari N. V., Sodré L., Stasińska G., Mateus A., Torres-Papaqui J. P., Schoenell W., 2007, MNRAS, 375, 16
Cox T. J., Jonsson P., Somerville R. S., Primack J. R., Dekel A., 2008, MNRAS, 384, 386
Dametto N. Z., Riffel R., Pastoriza M. G., Rodríguez-Ardila A., Hernandez-Jimenez J. A., Carvalho E. A., 2014, MNRAS, 443, 1754
de Grijs R., Lee J. T., Mora Herrera M. C., Fritze-v. Alvensleben U., Anders P., 2003, New Astron., 8, 155
Donzelli C. J., Pastoriza M. G., 1997, ApJS, 111, 181
Dors O. L., Copetti M. V. F., 2005, A&A, 437, 837
Dreyer J. L. E., 1888, Mem. R. Astron. Soc., 49, 1
Fairall A. P., 1979, MNRAS, 188, 349
Ferreiro D. L., Pastoriza M. G., 2004, A&A, 428, 837
Few C. G., Gibson B. K., Courty S., Michel-Dansac L., Brook C. B., Stinson G. S., 2012, A&A, 547, A63
González Delgado R. M. et al., 2015, A&A, 581, 103
Hernandez-Jimenez J. A., Pastoriza M. G., Rodrigues I., Krabbe A. C., Winge C., Bonatto C. G. S., 2014, Rev. Mex. Astron. Astrofis. Conf. Ser., 44, 178
Kewley L. J., Rupke D., Jabran Hahid H., Geller M. J., Barton E. J., 2010, ApJ, 721, L48
Krabbe A. C., Pastoriza M. G., Winge C., Rodrigues I., Ferreiro D. L., 2008, MNRAS, 389, 1593
Krabbe A. C., Pastoriza M. G., Winge C., Rodrigues I., Dors O. L., Ferreiro D. L., 2011, MNRAS, 416, 38
Krabbe A. C., Rosa D. A., Dors O. L., Pastoriza M. G., Winge C., Hägele G. F., Cardaci M. V., Rodrigues I., 2014, MNRAS 437, 1155 (Paper I)
Lambas D. G., Tissera P. B., Alonso M. S., Coldwell G., 2003, MNRAS, 346, 1189
Larson R. B., Tinsley B. M., 1978, ApJ, 219, 46
Lauberts A., 1982, The ESO/Uppsala Survey of the ESO(B) Atlas. Garching bei München: European Southern Observatory, ESO
Lauberts A., Valentijn E. A., 1989, The Surphace Photometry Catalogue of the ESO-Uppsala Galaxies. Garching bei München: European Southern Observatory, ESO
MacArthur L. A., González J. J., Courteau S., 2009, MNRAS, 395, 28
Martins L. P., Rodríguez-Ardila A., Diniz S., Riffel R., de Souza R., 2013, MNRAS, 435, 2861
Mateus A., Sodré L., Cid Fernandes R., Stasińska G., Schoenell W., Gomes M., 2006, MNRAS, 370, 721
Minchev I. et al., 2014, ApJ, 781, L20
Mishurov Y. N., Lépine J. R. D., Acharova I. A., 2002, ApJ, 571, L113
Mollá M., Díaz A. I., 2005, MNRAS, 358, 521
Morelli L., Corsini E. M., Pizzella A., Dalla Bontà E., Coccato L., Méndez-Abreu J., 2015, MNRAS, 452, 1128
Mulia A. J., Chandar R., Whitmore B. C., 2015, ApJ, 805, 99
Mullan B. et al., 2011, ApJ, 731, 93
Nikolic B., Cullen H., Alexander P., 2004, MNRAS, 355, 874
Osterbrock D. E., Ferland G. J., 2006, Astrophysics of Gaseous Nebulae and Galactic Nuclei, 2nd edn. University Science Books, Sausalito, CA
Pastoriza M. G., Donzelli C. J, Bonatto C., 1999, A&A, 347, 55
Patton D. R., Torrey P., Ellison S. L., Mendel J. T., Scudder J. M., 2013, MNRAS, 433, L59
Pilkington K. et al., 2012, A&A, 540, A56
Pilyugin L. S., Vílchez J. M., Contini T., 2005, A&A, 425, 849
Pilyugin L. S., Grebel E. K., Zinchenko I. A., 2015, MNRAS, 450, 3254
Rosa D. A., Dors O. L., Krabbe A. C., Hägele G. F., Cardaci M. V., Pastoriza M. G., Rodrigues I., Winge C., 2014, MNRAS, 444, 2005 (Paper II)
Rupke D. S. N., Kewley L. J., Chien L.-H., 2010, ApJ, 710, L156
Sánchez S. F. et al., 2012, A&A, 546, 2
Sánchez S. F. et al., 2014, A&A, 563, 49
Satyapal S., Ellison S. L., McAlpine W., Hickox R. C., Patton D. R., Mendel J. T., 2014, MNRAS, 441, 1297
Schlegel D. J., Finkbeiner D. P., Davis M., 1998, ApJ, 500, 525
Scudder J. M., Ellison S. L., Torrey P., Patton D. R., Mendel J. T., 2012, MNRAS, 426, 549
Sekiguchi K., Wolstencroft R. D., 1992, MNRAS, 255, 581
Woods D. F., Geller M. J., 2007, AJ, 134, 527
Wright E. L., 2006, PASP, 118, 1711

SUPPORTING INFORMATION

Supplementary data are available at *MNRAS* online.

Please note: Oxford University Press is not responsible for the content or functionality of any supporting materials supplied by the authors. Any queries (other than missing material) should be directed to the corresponding author for the article.

APPENDIX A: OBSERVED SLIT POSITIONS OF AM 1401–324

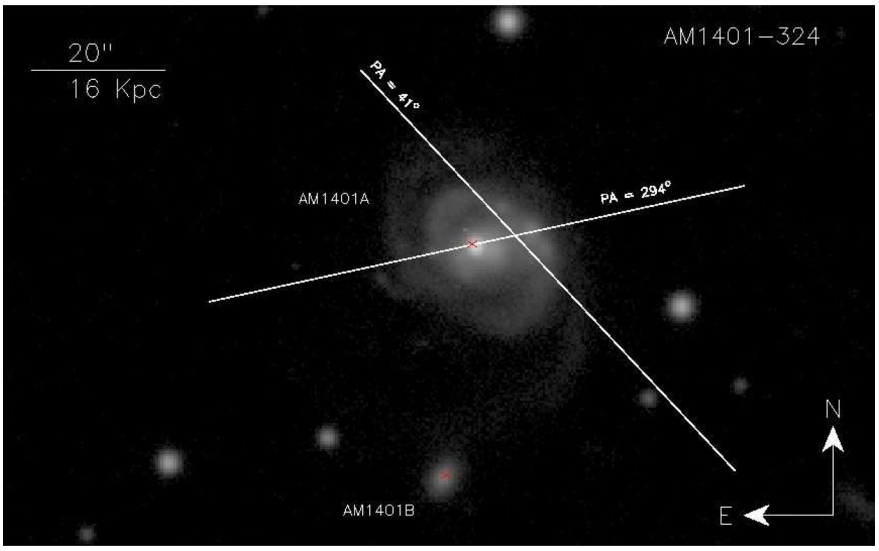

Figure A1. Slit positions for AM 1401–324, shown overimposed on the GMOS-S r' acquisition image.

APPENDIX B: REGIONS A AND B OF AM 2229–735

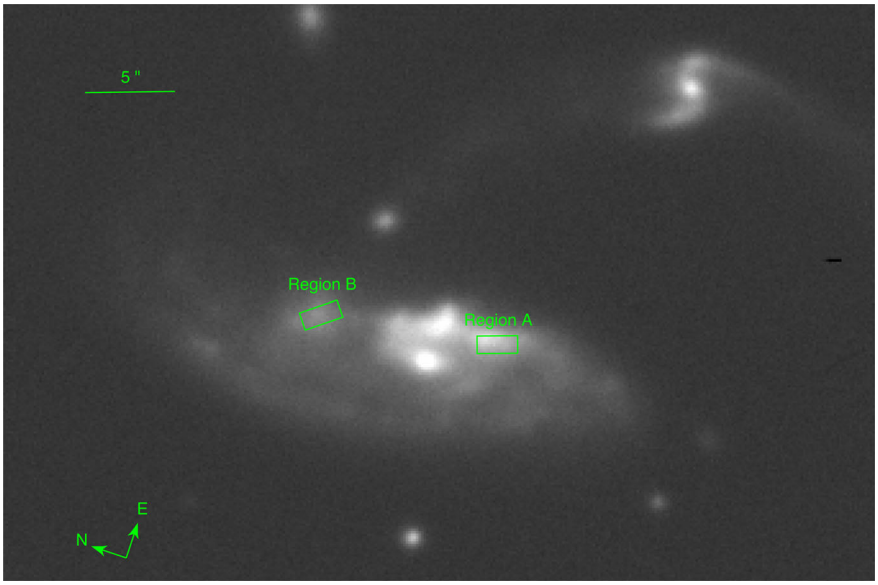

Figure B1. Image regions A and B of AM 2229–735, shown overimposed on the GMOS-S r' acquisition image.

APPENDIX C: LOGARITHM OF THE AVERAGE OF THE AGE OF THE STELLAR POPULATION

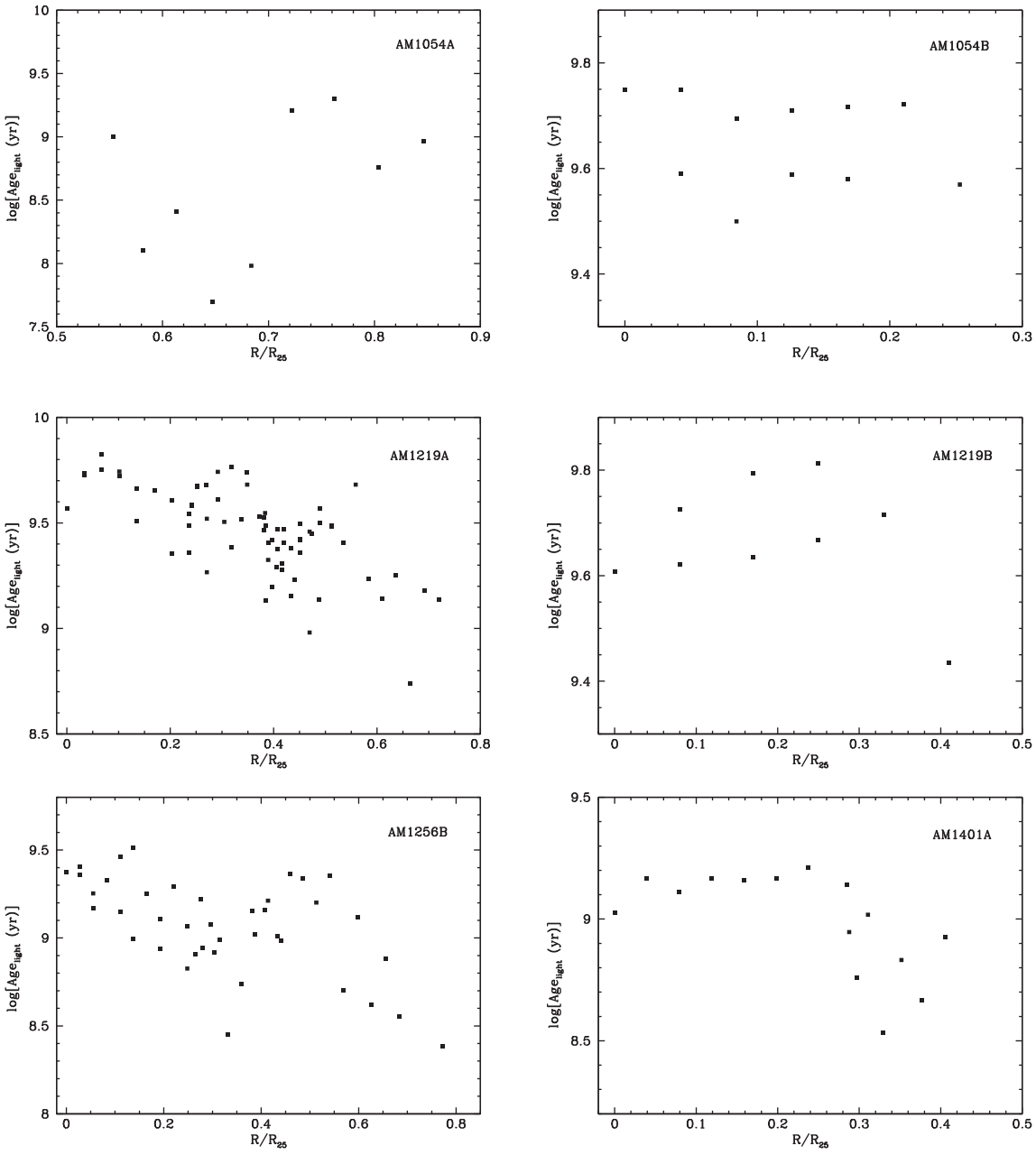

Figure C1. Logarithm of the average of the age of the stellar population (log[Age$_{light}$]) weighted by the flux contribution of each population versus the galactocentric distance R/R_{25} for the objects of our sample, as indicated. Points represent estimations for the regions along the disc of each galaxy.

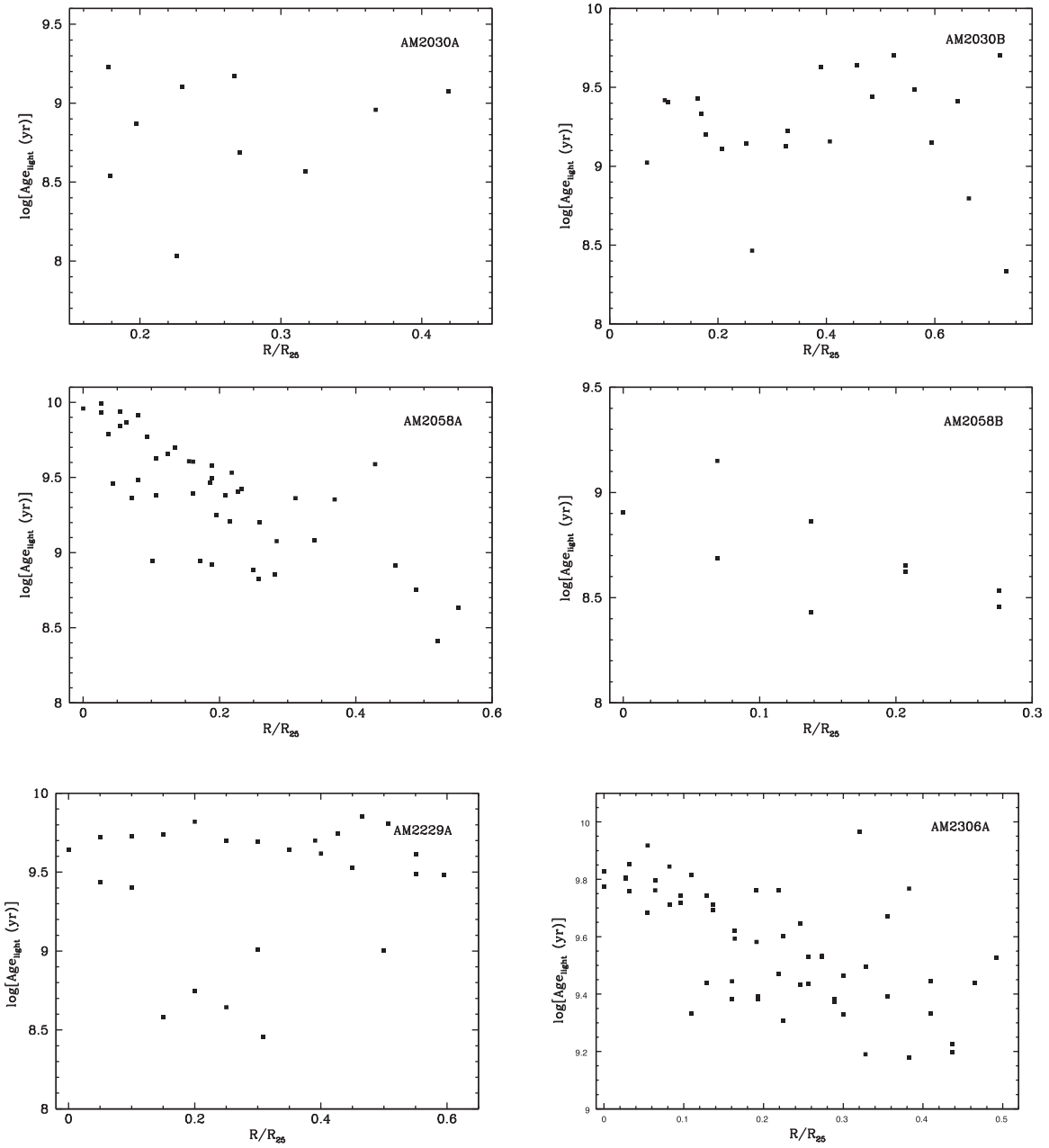

Figure C2. As Fig. C1, but for other objects as indicated.

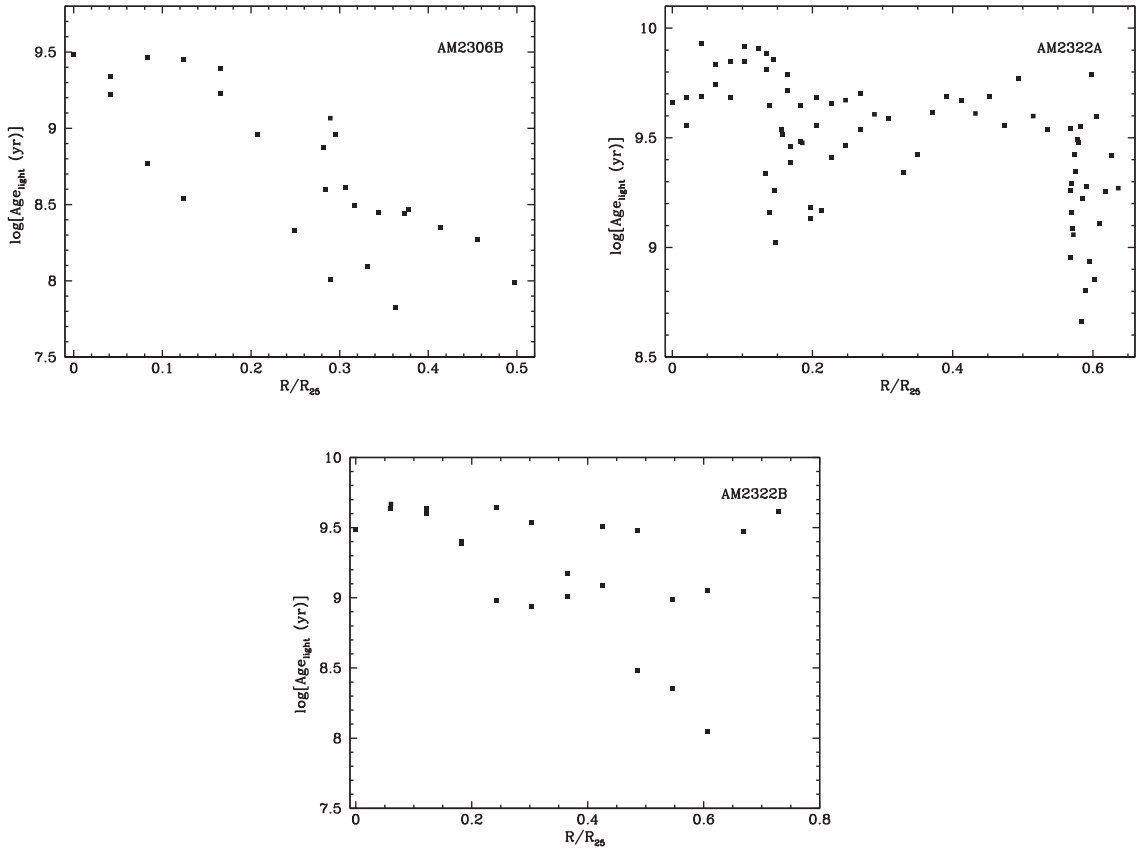

Figure C3. As Fig. C1, but for other objects as indicated.

APPENDIX D: GAS AND STELLAR PARAMETERS

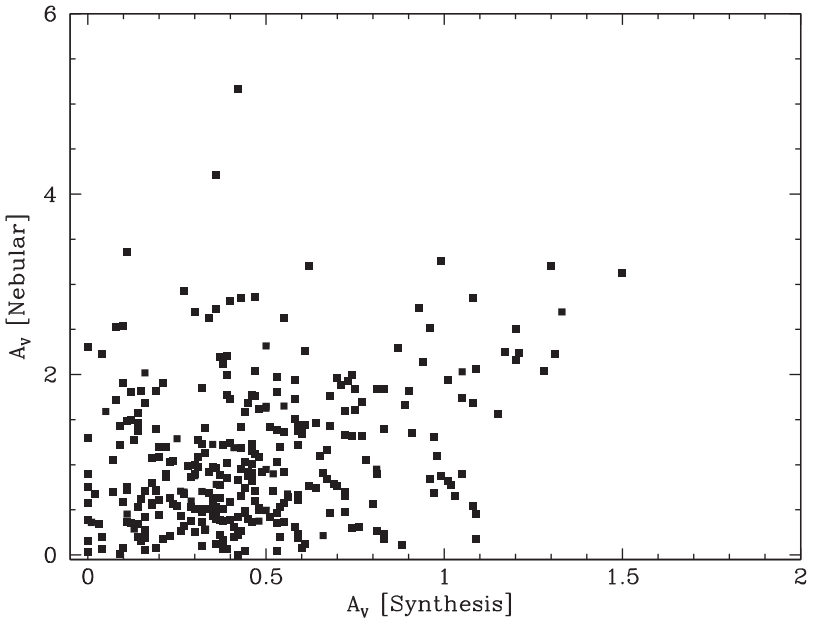

Figure D1. Comparison between extinction obtained from the stellar population synthesis (A_V[Synthesis]) and nebular extinction estimated from the Hα/Hβ emission-line ratio (A_V [Nebular]) for the objects in our sample.

APPENDIX E: GAS AND STELLAR PARAMETERS

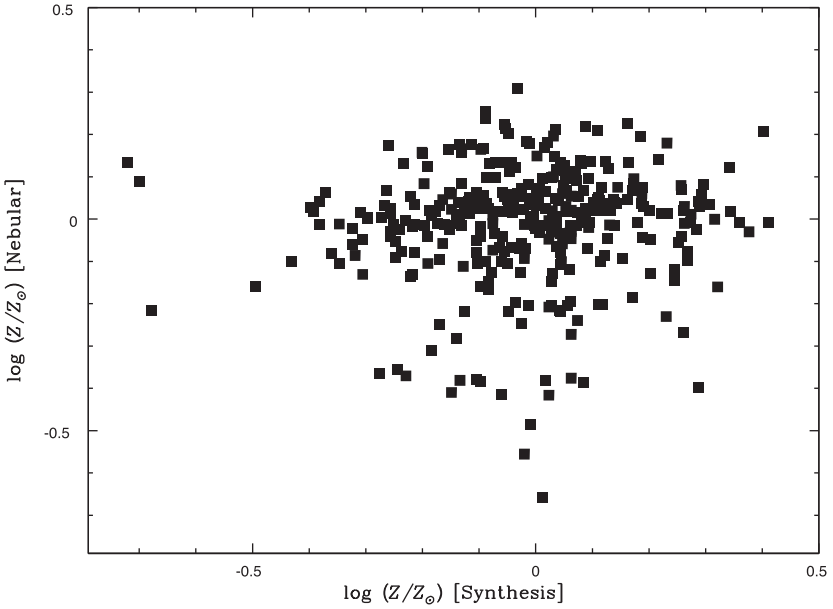

Figure E1. Comparison between stellar and nebular metallicities.

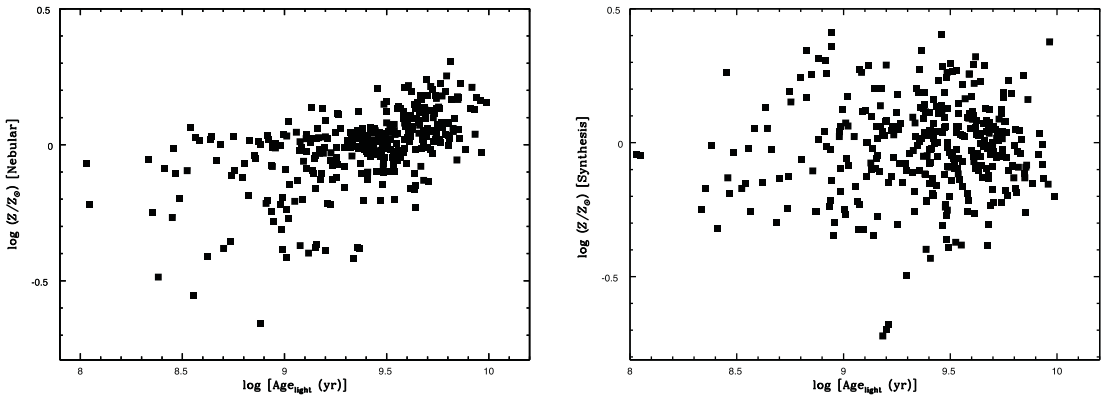

Figure E2. Comparison between stellar (left) and nebular (right) metallicities versus stellar age.

APPENDIX F: STELLAR POPULATION SYNTHESIS

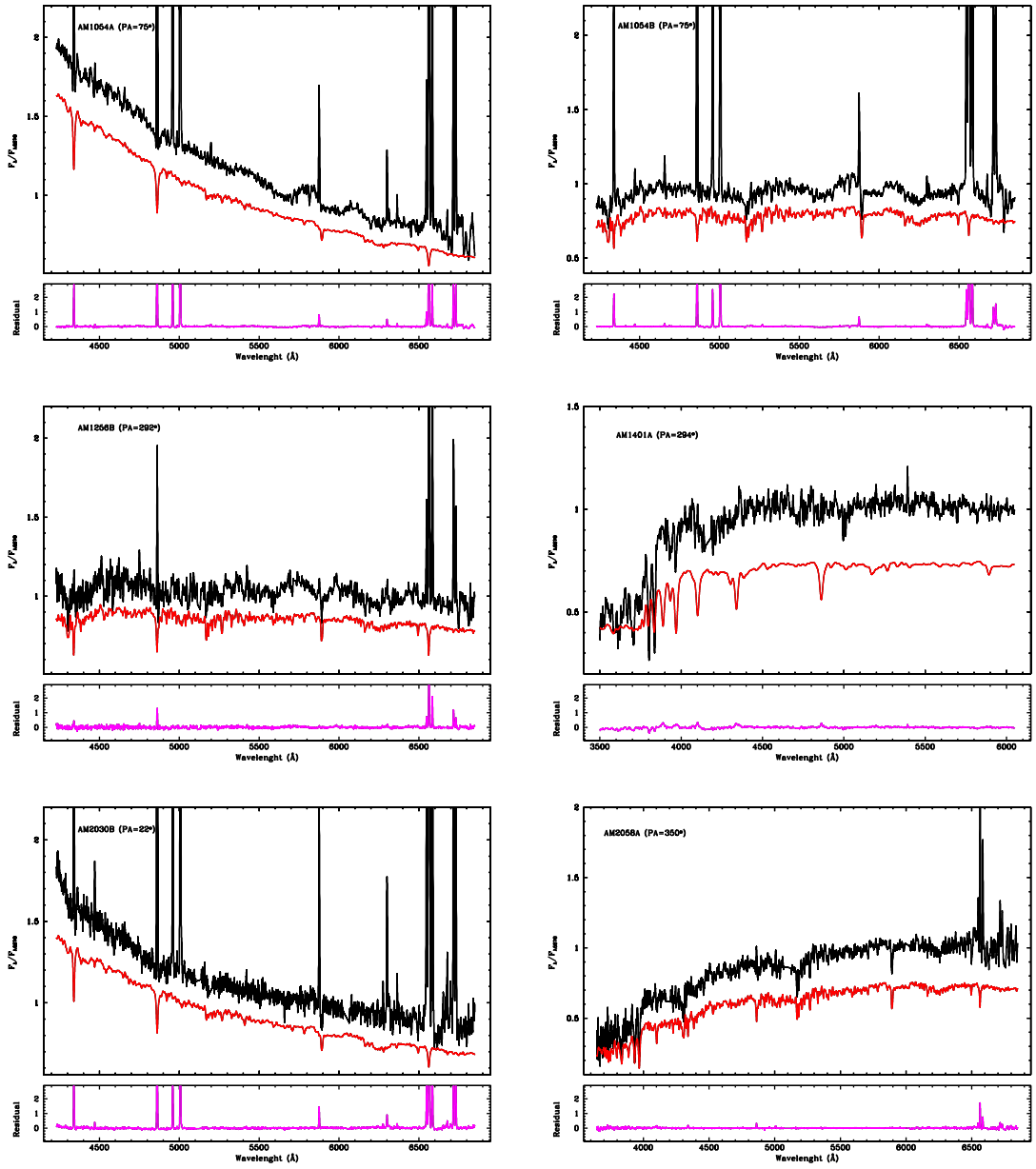

Figure F1. Stellar population synthesis for the nuclear regions of AM 1054A, AM 1054B, AM 1256B, AM 1401A, AM 2030B and AM 2058A. Top panel: the observed spectrum is plotted as a black line and the synthesized spectrum as a red line.The main absorption and emission features have been identified. Bottom panel: pure emission spectrum corrected for reddening.

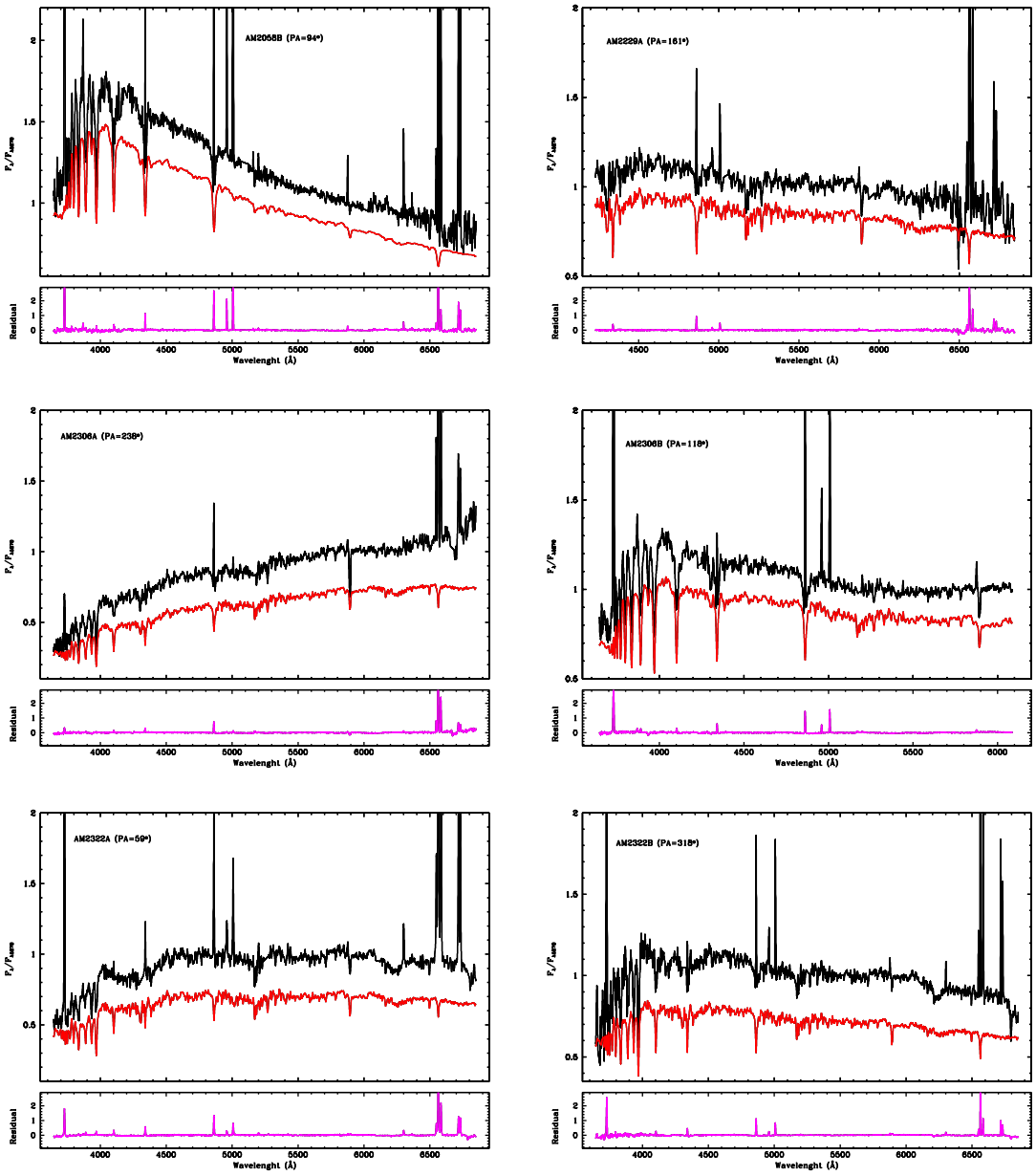

Figure F2. Same as Fig. 1, but for AM 2058B, AM 2229A, AM 2306A, AM 2306B, AM 2322A and AM 2322B.

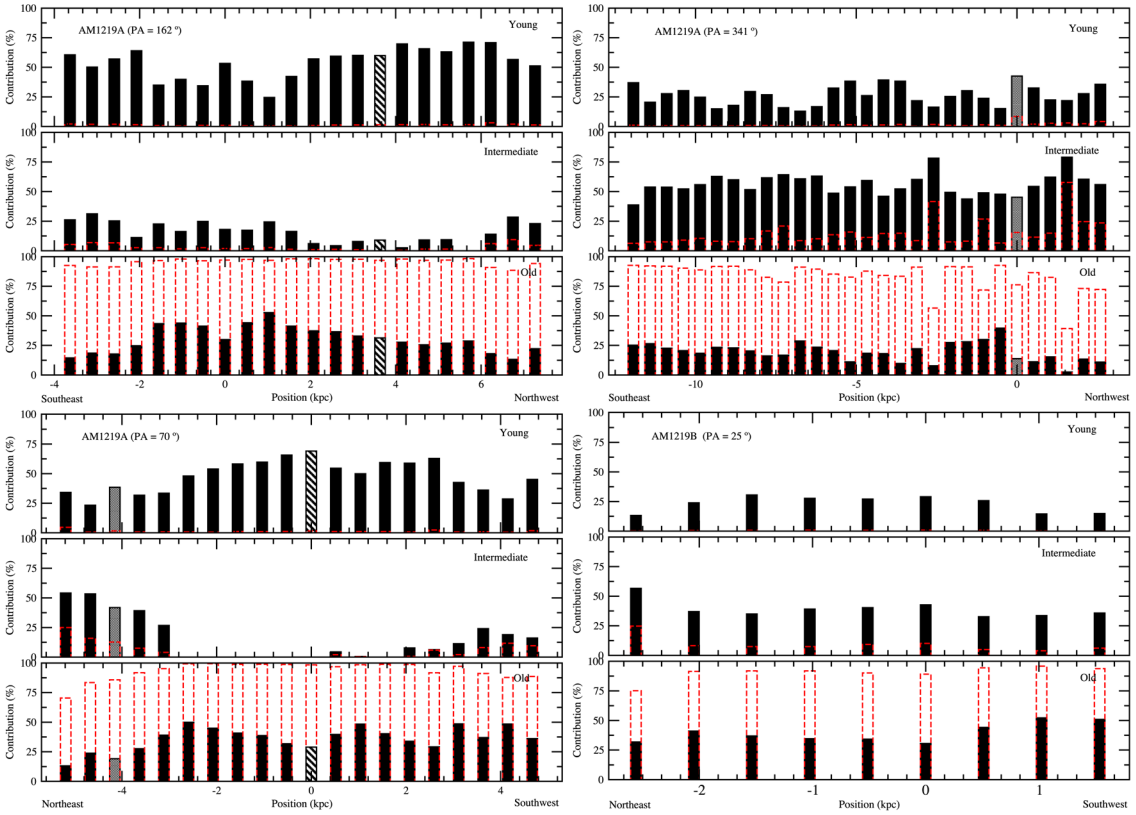

Figure F3. Same as Fig. 2, but for AM 1219A along PA = 162°, 341°, 70° and 25° for companion AM 1219B.

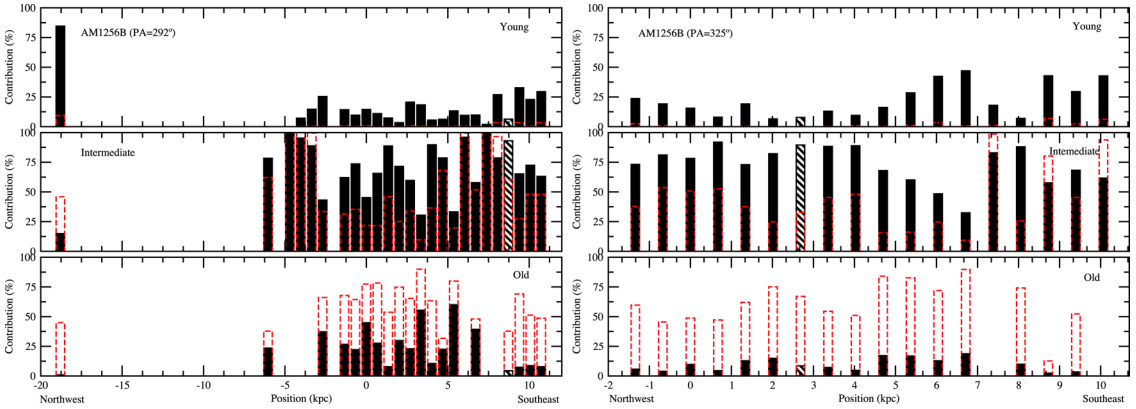

Figure F4. Same as Fig. 2, but for AM 1256B along the two slit positions observed.

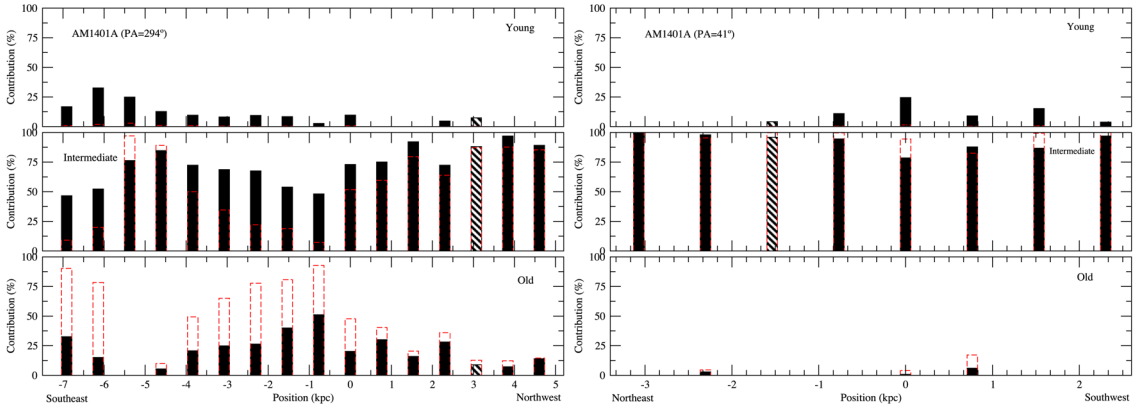

Figure F5. Same as Fig. 2, but for AM 1401A along the two slit positions observed.

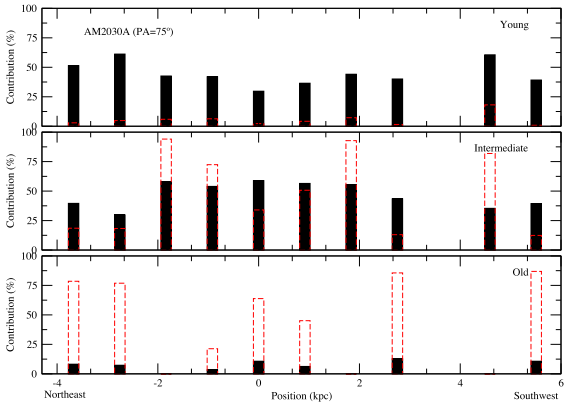

Figure F6. Same as Fig. 2, but for AM 2030A.

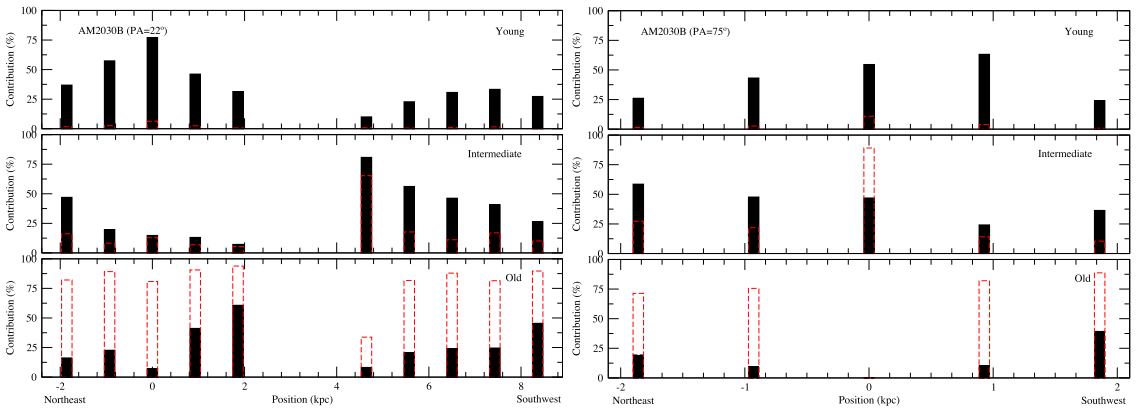

Figure F7. Same as Fig. 2, but for AM 2030B along the two slit positions observed.

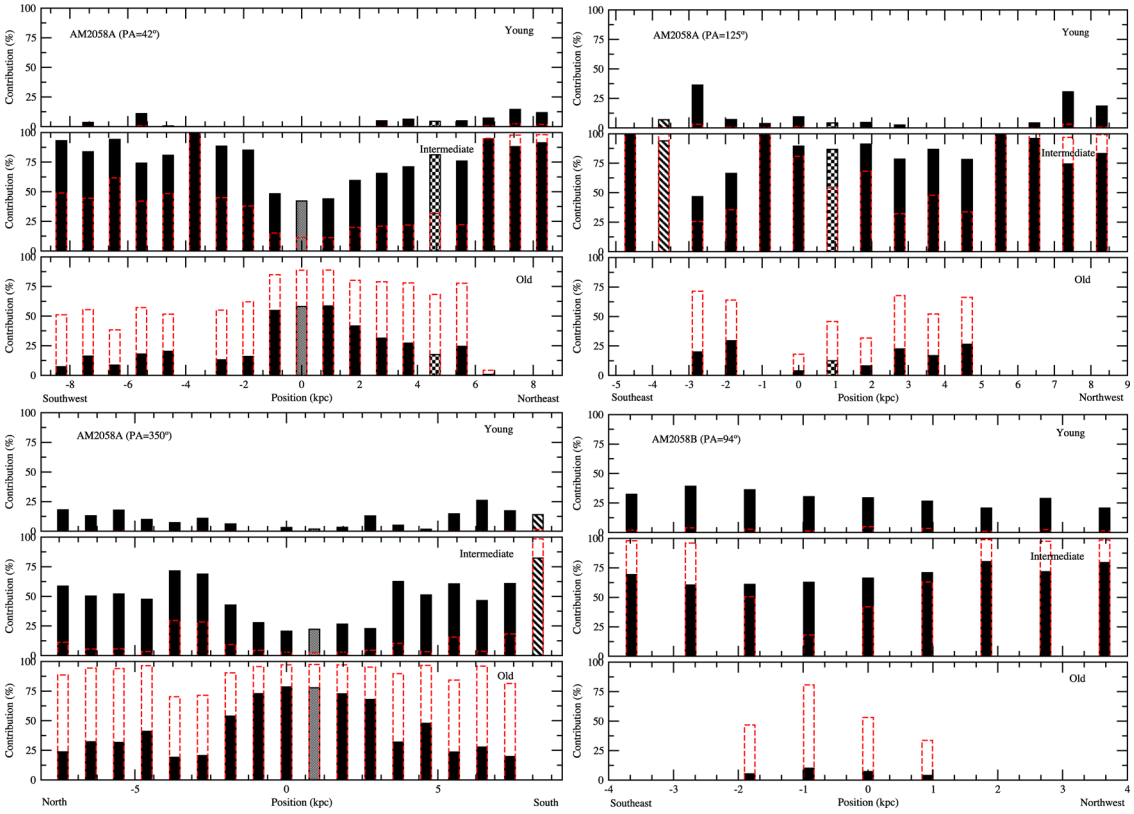

Figure F8. Same as Fig. 2, but for AM 2058A and AM 2058B (bottom right panel).

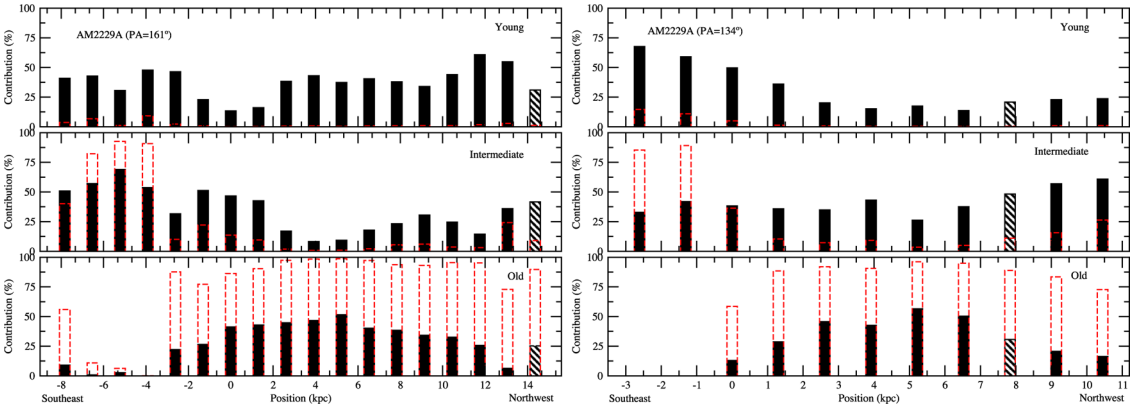

Figure F9. Same as Fig. 2, but for AM 2229A along the two slit positions observed.

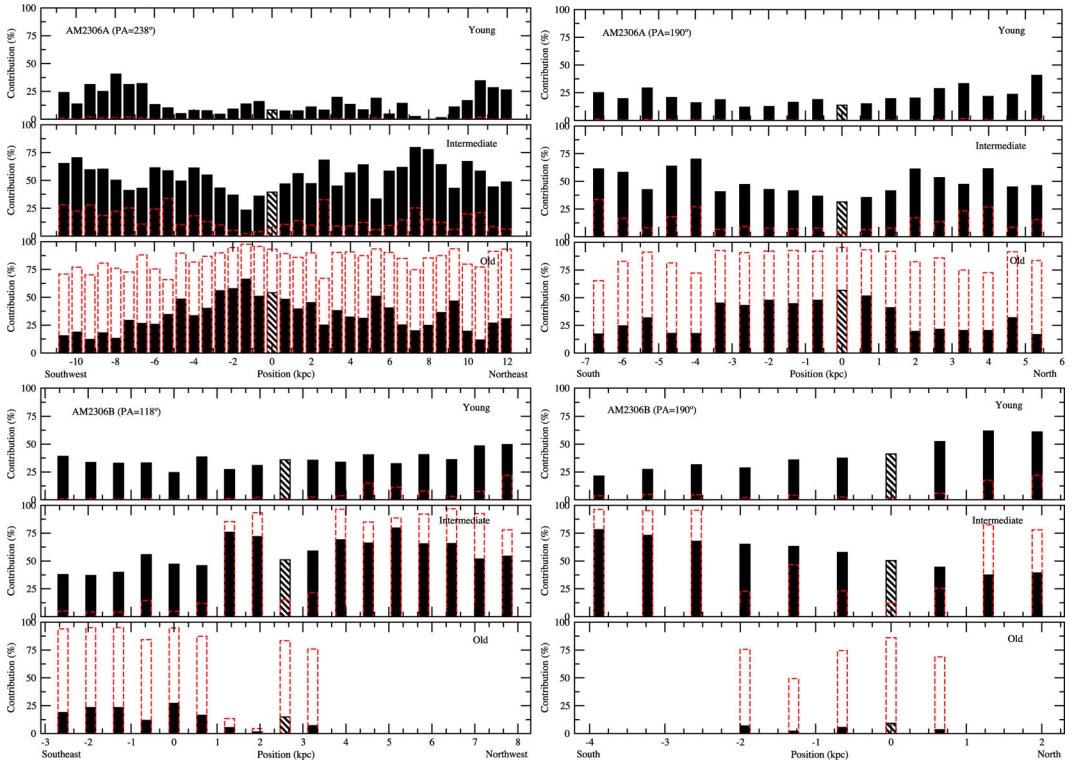

Figure F10. Same as Fig. 2, but for AM 2306A (top panels) and AM 2306B (bottom panels) along their corresponding slit positions.

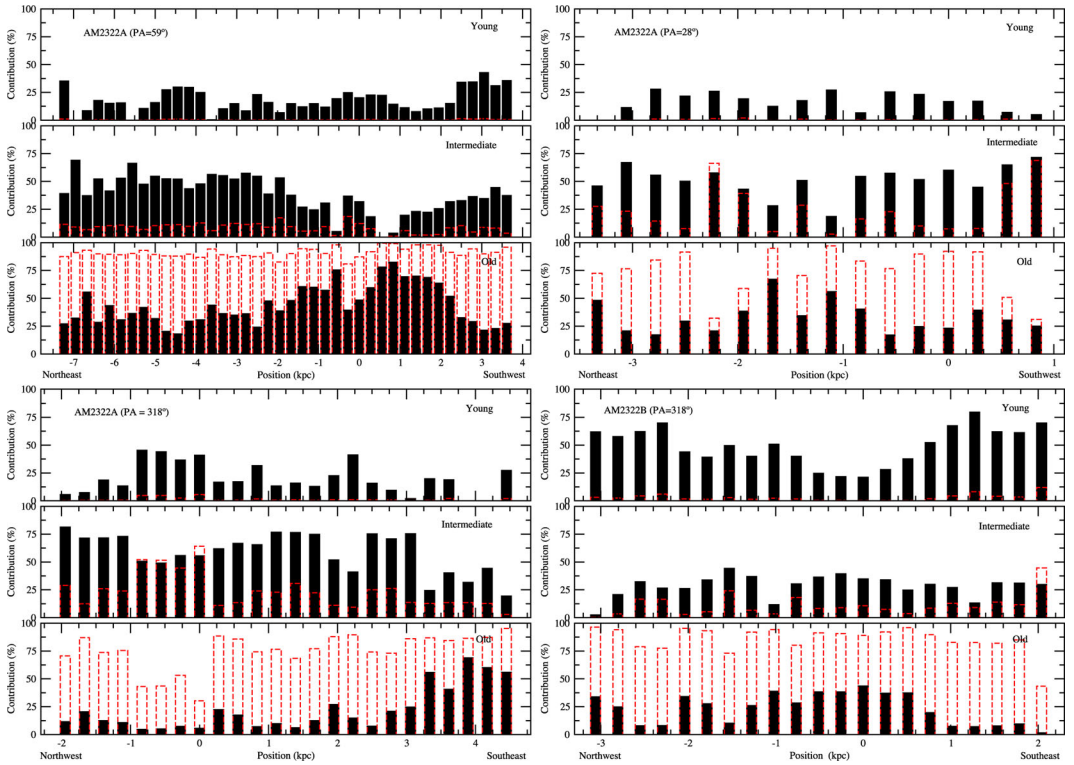

Figure F11. Same as Fig. 2, but for AM 2322A and AM 2322B.

This paper has been typeset from a TEX/LATEX file prepared by the author.